EXPERIMENTAL SURFACE HEAT FLUX MEASUREMENT IN HYPERVELOCITY FLOWS

BY

WILLIAM P. FLAHERTY

THESIS

Submitted in partial fulfillment of the requirements
for the degree of Master of Science in Aerospace Engineering
in the Graduate College of the
University of Illinois at Urbana-Champaign, 2010

Urbana, Illinois

Adviser:

Assistant Professor Joanna Austin

Abstract

Prediction of heat transfer is integral to development of hypersonic vehicles. Underprediction of heat transfer rates can result in catastrophic failures during flight testing. An example which illustrates the importance of heat transfer during hypersonic flight is the destruction of the space shuttle Columbia during the re-entry portion of STS-107. The shuttle experienced damage to its heat shielding, which in turn was not able to protect the craft from the extremely high levels of heat transfer experience during re-entry, resulting in the destruction of the craft. Due to both the high costs and dangers associated with flight testing, ground based experimental heat transfer data is essential the the design of safe and efficient hypersonic craft. Experimental data in facilities which have the ability to create mid to high enthalpy flowfields without large amounts of freestream dissociation is highly desirable in order to both validate CFD codes and to determine the effects of variations in geometry on heat transfer. The Hypervelocity Expansion Tube (HET) is one of a few facilities in the US that are able to create these flows, and thus it is an optimal test bed for these types of studies.

Two gage types used in order to measure surface heat transfer, thermocouples and thin film gages. This thesis details the development and application of thermocouples and thin film surface heat transfer gages in the HET. These gages have been extensively used in other hypersonic facilities, but their application and comparison in intermediate enthalpy conditions (like those created in the HET) has not been well established in previous reports. This study sought to compare the performance of the gages and to apply them to canonical model geometries to investigate heat transfer in the HET.

Acknowledgments

First and foremost I would like to thank my advisor Professor Joanna Austin. My success at the University of Illinois is due in large part to the help and support Professor Austin gave me throughout my graduate studies. Next, I would like to thank my parents, without whose help and support I would never be where I am today (you were right Mom, going to college was a good idea). I would also like to thank my fellow lab mates Ryan Fontaine, Manu Sharma, Andy Swantek, and Dave Prisco whose assistance both in and out of the lab has helped me immensely. I would also like to acknowldge the help of the Caltech T5 group including Prof. Hans Hornung, Bahram Valiferdowski, Drs Eric Marineau, Adam Rasheed, and Ivett Leyva for their valuable help with thermocouples. Thanks also to Lt. Col. Prof. Russell Adelgren for taking the time to discuss the construction of the thin film gages with me. Finally, thanks to my undergraduate advisor, Professor John Blandino. Without Professor Blandino I may never have been introduced to experimental research, and it was in his lab that my love for engineering was truly developed. This work was funded through the Air Force Office of Scientific Research FA9550-08-1-0172 with Dr. John Schmisseur as program manager.

Table of Contents

List of Tables

List of Figures

List of Symbols

c	Specific heat, kJ/kg-C
h	Enthalpy, J/kg-K
k	Thermal conductivity, W/m-C
p	Pressure, Pa
$\dot{q}$	Surface heat flux, W/m^2
t	Time, seconds
u	Velocity, m/s
x	Junction depth, m
K	Constant for gas composition
L	Length of plate, m
Le	Lewis number
M	Mach number
P	Prandtl number
R	Gas constant
Re	Reynolds number
T	Temperature, K
α	Thermal diffusivity, m^2/s
δ	Boundary layer thickness, m
μ	Viscosity, kg/m-s
ρ	Density, kg/m^2

Subscripts

e	Value in external flow
D	Quantity measured at formation
rec	Recovery value
s	Stagnation point value
w	Value at wall

Chapter 1

Introduction

Reliable prediction of the high heat transfer rates experienced during the hypersonic portion of planetary entry and descent is critical to vehicle survival. While non-intrusive diagnostics can be used to obtain temperature field data around models, wall-mounted sensors are commonly used to measure the heat flux at the surface. Two types of sensors which can be used for this purpose are coaxial thermocouple gages and thin film resistance thermometers. Individually, both types of gages have been used successfully in extensive studies at Calspan-University of Buffalo Research Center (CUBRC) [2, 3, 4, 5, 6, 7, 8, 9], NASA facilities [10, 11, 12, 13, 14, 15], Graduate Aeronautical Laboratories at Caltech (GALCIT) [16, 17, 18, 19], and the University of Queensland [20, 21], among others. Both thermocouple and thin film gages measure surface temperature from which heat transfer can be calculated. Both have μs response times, and can be flush-mounted in models. Coaxial thermocouples are robust, and can survive challenging experimental conditions. Thin film resistance gages typically provide improved signal levels, but are less robust, and have to be individually calibrated. As discussed below, thermocouples are generally preferred at higher enthalpy conditions, while thin film gages are used at lower enthalpy conditions. As a result, there are few studies which directly compare measurements from the two types of gages. In the present work, we perform experimental measurements at a range of intermediate enthalpies in hypervelocity flow and make direct comparisons between heat flux data obtained from thermocouple and thin film gages.

Hypervelocity flow conditions can be created using impulse ground testing facilities such as reflected shock tunnels (T5 at Caltech [22], HLG at the Institute of Aerodynamics and Flow Technology in Germany [23], LENS at CUBRC [24] and the 20 inch and 31 inch tunnels at NASA Langley [25]) and expansion tubes (X-series at University of Queensland [26], JX-1 at the Institute of Fluid Science in Japan [27], LENS-X at CUBRC [3]). In an expansion tube, the flow is accelerated by a shock followed by

an unsteady expansion wave. A range of test conditions can be relatively easily accessed by changing initial pressures and gas compositions, and thermochemical freezing, a common problem in facilities which utilize nozzles, is minimized. Facility disadvantages include reduced test times and increased viscous effects.

1.1 Literature Review

Miller [10] performed a comprehensive review of thin film gages used in the NASA Langley Continuous Flow Hypersonic Tunnel (CFHT), comparing their performance to thick-skin calorimeters. Gage durability on both glass and ceramic substrates were tested. It was found that of the four glass substrate models, only one survived longer than one test. The ceramic models fared slightly better, with one surviving six tests, and the other surviving all nine tests it was subjected to. Since these tests were conducted in a continuous-flow facility the gages were exposed to test times three orders of magnitude longer than typical impulse facility test times. The method used to apply the gages to the substrate was significantly different than the current technique which could have significant effects on gage durability. Chadwick [8] performed a detailed review of the use of thin film heat transfer gages in the CUBRC 96 inch reflected shock tunnel facility. Heat transfer data are obtained at multiple run conditions with enthalpies ranging from 1.85 to 7.44 MJ/kg and Mach numbers from 10 to 16.

Kidd presents a detailed survey of the coaxial thermocouples used at Arnold Air Force Base, as well as many other facilities [11]. Some issues associated with the coaxial gages are quantified. The two major conclusions from this study were that coaxial thermocouples can be utilized at test times much longer than semi-infinite body assumption would allow, and also that the gage length does not need to be equal to the model wall thickness. In a later study, Kidd et al. investigated the effects of extraneous voltages caused by electrical connections between the model and the gage, and found that care must be taken to minimize the effects of such contact [12].

Coaxial thermocouple gages are typically used in high stagnation enthalpy flows in the Caltech T5 reflected shock tunnel facility. Sanderson [16] originally developed a new coaxial thermocouple design in order to avoid fragility issues associated with thin film gages, and other issues with the more generally used coaxial wire thermocouples. Sanderson found that extraneous voltages produced from contact between the

gage and the model were negligible with the new design. These thermocouples have been applied to other experiments in the T5 facility [17, 18, 28]. Marineau and Hornung [29] performed a numerical study of the gages designed by Sanderson. The response time and accuracy of the gages was found to be strongly dependent on the junction geometry. A simultaneous calibration procedure for multiple gages is proposed if individual calibration is desired.

Salvador et al. report on the development of coaxial thermocouple gages for use in the shock tunnel facilities at the Laboratory for Aerothermodynamics and Hypersonics in Brazil [30]. One important result from this paper is the demonstration of the dependence of gage response time on the connection properties between the two electrodes. It was found that simply by using different grit sandpaper to create the junction the response time could change by a factor of two.

While not focused on direct comparative measurements, there are a limited number of studies in which both thin film and thermocouple surface heat transfer data are available. In a recent study at the National Aerospace Laboratory in Japan, both coaxial and thin film thermocouples were used to compare the operation of the Hypersonic Wind Tunnel, the High Enthalpy Shock Tube, and the Hypersonic Shock Tube to establish guidelines for the use of the facilities [31]. The thermocouple data was found to be in good agreement with IR thermography, and the non-dimensional heat transfer agreed to within a few percent between all three facilities. Both thin film and thermocouple gages were used in two recent studies at CUBRC. The first study focused on real gas effects in both the LENS I and LENS X facilities for test gas enthalpies from 2 to 12 MJ/kg [4]. Heating rates measured by both gages were in good agreement with each other, however at high enthalpies the measured heat flux did not agree with either fully catalytic or non-catalytic wall predictions. The second study at CUBRC, conducted in the LENS I reflected shock tunnel, used the gages to investigate the role of catalytic effects on a sphere-cone model in both nitrogen and carbon dioxide. Tests were run at test gas enthalpies of 2, 6, and 8 MJ/kg. This study found good agreement between the gages, but found that all gage types measured heating levels higher than predicted assuming a non-catalytic wall, but less than that predicted assuming a fully-catalytic wall [5].

Though these sensors have been used extensively for many years, their selection has relied on very general distinctions, where thin film gages are used for “low” enthalpy conditions, and coaxial

thermocouples are used for “high” enthalpy conditions. In order to develop a more rigorous method for application of the gages, properties such as signal-to-noise ratio, durability, accuracy, and wall catalysis effects must be quantified for a range of flow enthalpies. Creating a database of these properties would allow researchers to determine the best gage for their application, and increase confidence in surface heat transfer measurements. This thesis details the initial design and application of the gages for use in the HET. Also, the results collected with both gages are compared for simple model geometries in order to determine if any discrepancies exist between the gages.

Chapter 2

Experimental Setup

The Hypervelocity Expansion Tube (HET) is an expansion tube facility at the University of Illinois which operates across a range of Mach numbers from 3.0 to 7.5 and stagnation enthalpies from 4.0 to 8.0 MJ/kg [32]. Heat flux data can be obtained using both thermocouple and thin film gages in this facility, allowing direct comparisons to be made between the two measurement techniques. The 9.14 m long facility consists of driver, driven, and accelerator sections all with a 150 mm inner diameter. The driver and driven section are separated by a metal diaphram, while the driven and accelerator sections are separated by a thin plastic diaphragm. Test conditions can be changed simply by changing the fill pressures and gases in the three sections of the tube. Theoretically, any test gas could be used in the driven section. Air, CO2, and Argon have all been used as test gases in the HET. Accelerator gas is also varied depending on the run condition, and is typically helium or air [32].

Operation of the tube begins by bringing all three sections to different pressures. The driver section is bought down to vacuum (around 200 mtorr), the driven section is brought to a pressure typically between 1 to 6 kPa, and the accelerator section is brought to a pressure of a few hundred mtorr. This process is done iteratively in order to avoid rupturing the thin secondary diaphragm (which can tolerate approximately a 20 kPa difference in pressure between sections). The pressures in the driven and the accelerator sections are varied based on what run condition is desired for that shot. Once all three sections are at the required pressure, the driver section is pressurized to around 2.5 MPa, causing the primary diaphragm to rupture. This is referenced as time zero on the x-t diagram shown in Figure 2.1. This high pressure ratio across the diaphragm causes a shock to propagate through the driven section, causing mass movement in the test gas. After the initial shock has passed through the test gas, the test gas is at condition two (indicated on the x-t diagram). When this initial shock reaches the secondary diaphragm it ruptures it instantly (due to its

thinness). This results in a transmitted shock which propagates through the accelerator section (inducing mass motion in the accelerator gas, indicated as condition six in the x-t diagram), as well as an unsteady expansion fan. The gas in the driven section (known as the "test gas") is accelerated through this expansion fan to hypersonic velocities (indicated as condition seven on the x-t diagram). From the perspective of a model mounted in the test section of the HET, it first experiences the transmitted shock created by the rupture of the secondary diaphragm. This shock is followed by the accelerator gas, which has been put in motion by the transmitted shock. Next comes the contact surface between the accelerator gas and the test gas. While theoretically this should be a discontinuity there will be finite time over which it spans. Following the contact surface will be the test gas. The time during which the model is exposed to the test gas is denoted as the "test time". Termination of the test time occurs when the tail or the reflected head of the unsteady expansion wave reaches the test section. In run conditions used in the HET it is most commonly the expansion tail which arrives in the test section first and terminates the test time, but it is theoretically possible to create a run condition which is terminated by the expansion head. Finally, the driver gas passes over the model. This portion of the shot is the most mechanically stressful to the model as the driver gas has a stagnation pressure that is theoretically equal to the pressure it was at when the primary diaphragm burst (since the gas was stagnated at that time). Thus, when determining the forces exerted on the model (in order to design it to be safe to mount in the tube) the burst pressure of the diaphragm should be used as the highest pressure exerted on the blunt faces of the model. A typical pitot probe trace, spanning from the arrival of the initial shock to the termination of the test gas, is shown in Figure 2.2, and a picture of the HET facility can be seen in Figure 2.3.

For this study, three test conditions with different stagnation enthalpies were selected. Invicid, perfect gas dynamic calculations are used to predict test gas conditions, shown in Table 2.2. Previous to the beginning of this experiment the HET had two well characterized run conditions, which are now designated as Air-5 and Air-6. Both of these run conditions are low Reynolds number and low density conditions. Since the HET has the ability to access a range of run conditions it was decided to investigate run conditions that would have an increased Reynolds number and density than those of the Air-5 and Air-6 cases. This would also create a run condition which would have a higher probability of transitioning to turbulence in the

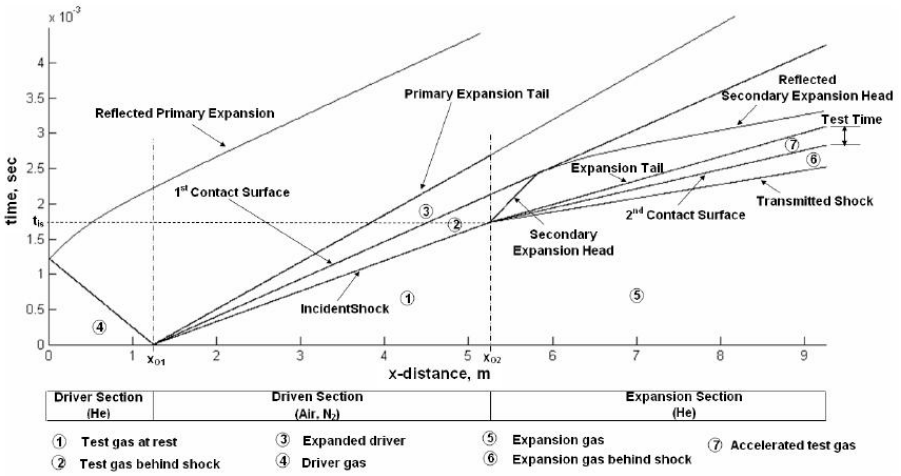

Figure 2.1: Sample x-t diagram for HET operation [1]

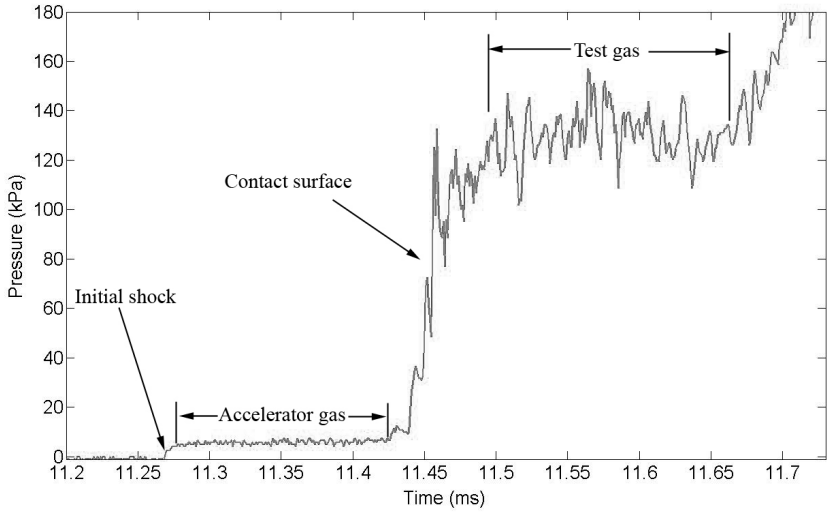

Figure 2.2: Sample pitot trace in the HET

presence of a trip (a future goal of this work). Three run conditions were initially studied, and their properties are shown in Table 2.1.

While both the Reynolds number and density of these shots were in the desired range, they displayed extremely high levels of free stream noise throughout the test gas, making them unusable. An example pitot trace from one of these shots (centered in the time around the test gas) can be seen in Fig 2.4. It is believed that the noise in the test gas is a function of the ratio of the gas density between the driver and driven sections [33]. Thus, the only was to reduce noise is to reduce the driven pressure (since the burst pressure of

Figure 2.3: HET facility

Table 2.1: High-density run conditions

Test Gas	Accelerator Gas	M_∞	T (K)	h_0 (MJ/kg)	Re/m	Static P (kPa)
Air	He	6.08	564.1	4.75	2.65X10^6	4.30
CO2	He	6.94	626.3	4.20	2.75X10^6	3.84
Ar	He	6.23	582.5	4.23	1.98X10^6	4.07

the driver is set by the knife blades and diaphragm). Unfortunately, reducing the driven pressure (and therefore the accelerator pressure) to maintain the same run condition will result in much lower densities, and therefore lower Reynolds numbers. In order to try to alleviate this problem, it was decided to run the lower driven and accelerator pressures, but change the accelerator gas to match the test gas. This resulted in a higher Reynolds number and density, but comes with an associated decrease in Mach number due to the decreased sound speed ratio across the driven and accelerator sections. Trial shots were run at this new condition using air as both test and accelerator gas, and the pitot traces indicated a long, stable test time. Another parametric study was undertaken to determine a run condition with a suitably high Mach number and acceptable Reynolds number. A new run condition, designated Air-4, was found that satisfied both

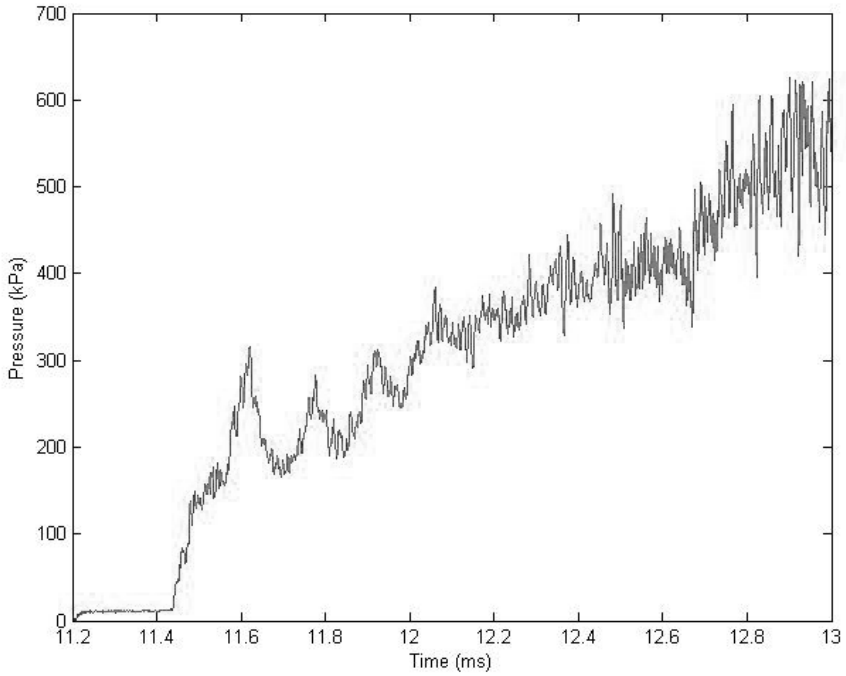

Figure 2.4: High density test gas pitot trace.

requirements. Its parameters are presented in Table 2.2 along with those of Air-5 and Air-6. The Mach number and enthalpy of Air-4 lie on the mid and low ends of the tubes capabilities respectively. Air-5 is a variation of the original main run condition in the tube. It was re-classified from Air-1 to Air-5 when the burst pressure of the primary diaphragm was lowered, which resulted in a slight change in the run condition. Air-5 is a low density, low unit Reynolds number condition, and has a Mach number and enthalpy that lie on the higher end of the tubes capabilities. For this condition helium is used as the accelerator gas. Air-6 is also a low density, low unit Reynolds number condition, but it's Mach number and enthalpy lie in the mid-rage of the tubes capabilities. Air-6 utilizes helium as the accelerator gas.

2.1 Thermocouple Development

Surface mounted thermocouples are very common sensors used for the measurement of the surface temperature histories in impulse facilities. Thermocouples operate using the Seebeck effect, which states that when two dissimilar metals are joined there is a measurable voltage difference between the two wires

Table 2.2: Theoretical parameters for HET run conditions.

Condition	Air 4	Air 5	Air 6
Mach number	5.12	7.45	5.73
Static temperature, K	676	642	909
Static pressure, kPa	8.13	0.77	1.86
Velocity, m/s	2664	3779	3457
Density, kg/m^3	0.042	0.004	0.007
Test time, μs	361	163	242
Unit Reynolds number, $1/m$	3.42E6	0.50E6	0.63E6
Stagnation Enthalpy, MJ/kg	4.08	7.65	6.70
Initial Pressures, kPa			
Driver section	2500	2500	2500
Driven section	6.0	1.5	1.2
Expansion section	0.08	0.02	0.07

which changes with temperature [34]. One of the most basic and widely used thermocouple designs is two wires with different composition joined together using either a simple solder or a weld. While these types of thermocouples are extremely robust and easy to manufacture, they suffer from slow response times and the inability to be surface mounted. Due to the short test times in impulse facilities as well as the desire to get surface data, it is necessary to develop new thermocouple designs to overcome these problems. Since the early 1950's, many impulse facilities have utilized coaxial wire thermocouples. These gages are constructed out of a thin tube of one electrode material, and a solid wire of the second electrode material. The solid wire is drawn through the tubular electrode, and insulated from it by a thin lair of an electrically insulating material. The gage is then installed in a model such that the surface of the gage is parallel with the surface of the model. The top of the gage is then sanded. During this sanding process, strands of the metal from the inner electrode are brought into contact with the outer electrode, creating the thermocouple junction [12]. This sanding process is extremely important to the eventual properties of the gage (such as response time). While this design overcomes the issues of typical thermocouples, it is not without drawbacks. The junction created by sanding can result in inconsistent gage response times, and the long lengths of the gages can cause them to act as antennas, picking up ambient electrical noise. The thermocouples used in these experiments are based on the design of Sanderson [16]. These thermocouples were designed specifically to avoid the issues with the more common coaxial wire thermocouples. They are coaxial, 2.4 mm in diameter, type E (Constantan-Chromel), and mount flush with the surface of a model. The two coaxial elements are

designed such that an extremely thin junction (on the order of 1 μm) is formed at the surface. An image of these two electrodes compared to a penny can be seen in Figure 2.5.

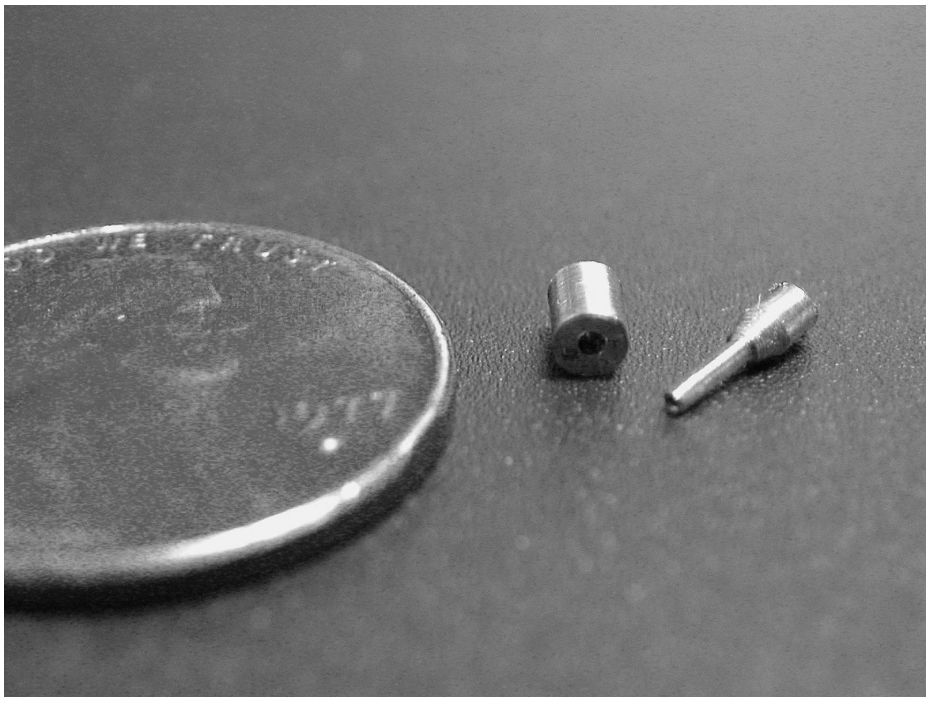

Figure 2.5: Thermocouple electrodes.

This type of thermocouple gage is used extensively in the T5 reflected shock tunnel at GALCIT [16, 17, 18], where the high enthalpy test conditions result in adequate signal levels and the robust design of the gages make them highly resistant to damage caused by particulates in the test gas as well as the large heat fluxes [16]. Technical drawings of the thermocouples, as well as advice on their construction, was provided by the T5 group at Caltech. Initially, it was attempted to make the thermocouples completely in house at the University of Illinois. To aid in this purpose a MicroLux variable speed bench lathe was procured. The appropriate equipment was purchased so that the small thermocouple elements could be properly mounted in the chuck. The type E thermocouple material was purchased from Omega Engineering. Initial attempts to manufacture the thermocouples resulted in multiple setbacks. The larger outer electrodes proved relatively easy to machine, but the much smaller inner electrodes proved to be extremely difficult, and very few survived the machining process. The small "stem" of the inner electrode had an outer diameter of only 0.025 inches, and it was found to be extremely difficult to make this cut on the lathe without bending the stem at the same time. During this period a series of guidelines for making the gages was developed:

1. Sharp, hand-ground tools were most effective, and it was imperative to keep a large supply of freshly sharpened tools.

2. When aligning the tool, care was taken to ensure that the cutting edge would hit the stock first, otherwise the small stock may bend away.

3. When taking cuts for the electrodes the entire cut was taken in one pass. While this may result in a non-optimal surface finish, repeat passes increase the chance of the electrode bending.

4. When using small drill bits the bit was brought as close to the stock as possible with the slide, and the hand wheel was kept loose. This helped to prevent the small bit from breaking.

5. Go slow with both RPM and feed rates. The RPM was set to approximately 140 to drill and 240 to turn the thermocouple material.

6. A small amount of play was allowed for in the slides (especially the angle slide). If the slides were kept too tight the stock had a higher chance of bending during the machining process.

A small number of working thermocouples were developed during this phase of the project. These thermocouples were installed in a stagnation sphere and tested in the HET. Though the signals obtained were far too noisy to be of practical use, the signal level was good enough to confirm that the thermocouples would be usable in the HET. Due to the extremely large time commitment required to produce the thermocouples it was decided to farm the machining work out to a machine shop which specialized in producing small parts, and keep the assembly of the individual thermocouples in house. It was decided to use Pacific Precision Inc. in California as they are the same machine shop used by the Caltech T5 group, and therefore already had experience manufacturing these thermocouples. Though the cost per thermocouple was higher than producing them in house, it was still substantially lower than if the gages had been bought commercially. Once the two electrodes have been made (whether in or out of house), they must be assembled in a specific way in order to ensure gage functionality as well as the proper response time. The two electrodes must be joined together using a layer of epoxy in order both to mechanically hold them together as well as insulate the electrodes from each other at all locations other than the surface junction.

Also, when joining the two electrodes together they must be pressed together with enough force to create the surface junction, but not too much force so that it causes the sharp contact point between the two electrodes to deform. This deformation can result in problems with response time and signal level. A special form was designed and machined in order to hold the two electrodes together while the epoxy dried. An illustration of an ideal junction can be seen in Figure 2.6.

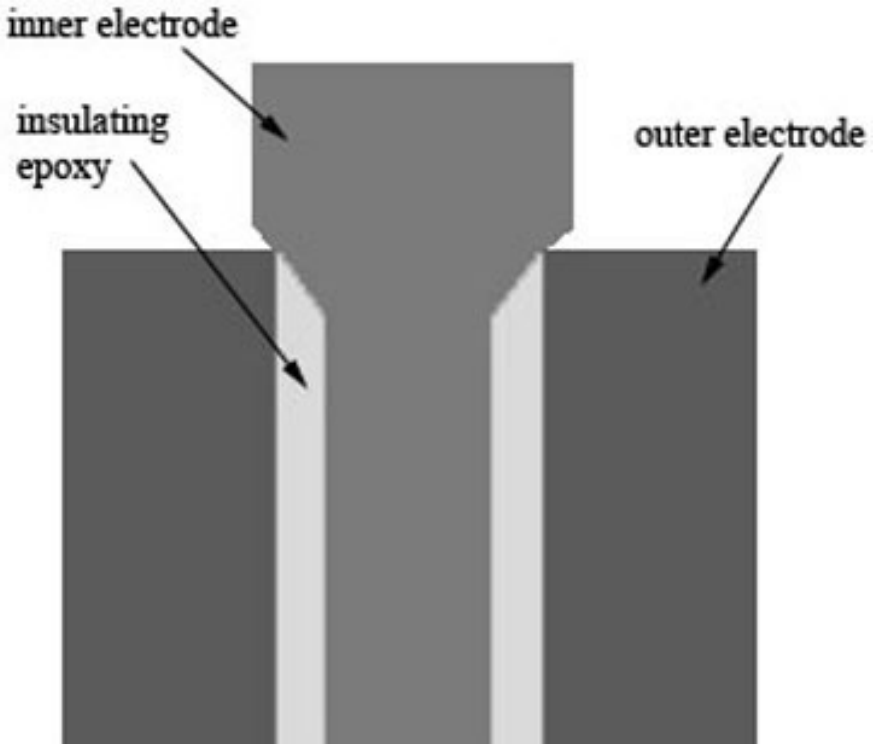

Figure 2.6: Sketch of thermocouple junction.

Secondly, wires must be soldered to each individual electrode so that the signal from the junction can be fed out of the test section. This soldering process is extremely delicate, as the wires are 30 gage and the holes are of a correspondingly small diameter. Care must be taken to ensure that the solder junction is strong and that the two electrodes are not soldered together. The first method developed to assemble the thermocouples involved epoxying the two electrodes together first, waiting for the epoxy to dry, and then soldering the wires to the electrodes. This introduced one major problem to the construction process. It was necessary during the soldering process to keep the soldering iron at almost the max temperature possible. If the iron was in contact with the electrode for too long it could result in a softening of the epoxy joining the electrodes, causing the junction between the two electrodes to fail. This resulted in a broken thermocouple

which must be thrown away. It was later determined that the wires could be soldered to the electrodes before they were joined using the epoxy. This eliminates the issue encountered previously and resulted in a much higher thermocouple survival rate. The form for holding the drying thermocouple had to be slightly modified to allow this new method, but this modification posed no issues. After the two electrodes are joined together and the wires are soldered to the back, a small bead of epoxy is placed on the back of the thermocouple to add support to the solder junctions. Once the epoxy bead has dried the thermocouple is ready for installation in the model. The thermocouple is inserted (wire first) through the top of the model. Next, its sides are coated with a thick layer of super glue and it is inserted into the model. A razor blade is used to align the top of the thermocouple with the top of the model. Once the super glue has dried, the protruding pin is removed using a fine tooth jewelers saw and the thermocouple is filed until it is flat with the surface of the model. Finally, 500 grit sandpaper is used to sand the junction. Multiple sandpaper grits were tested and 500 grit was found to produce the most consistent thermocouple response. Throughout the entire assembly process, it is useful to check the resistance between the two wires at every stage. A good, working thermocouple will typically have a resistance between 0.9 and 1.4 Ohms. Unfortunately there is no way to determine the response time of a thermocouple before it has been used in a test in the HET. A preliminary way to check the response time is a visual inspection of the junction after installation. The thermocouple should lie almost flat with the surface, and the junction should be highly polished. It should be difficult to to see the line between the two electrodes. The best way to determine if the gage response time is high enough is to check the gage's response to the incident shock in the HET. If the gage registers an almost discontinuous change in temperature as a result of the shock passage then it can be considered to have a high enough response time.

The signal is fed out of the test section through a 42 pin KF50 flanged feedthrough from Kurt J. Lesker (part number IFTRG417018C). On the vacuum side the thermocouple wires are soldered to individual female D-sub connector pins. On the air side, custom cables are used to connect the feedthrough to the signal conditioners. These connectors are made of RG58 coaxial cable. On one end the signal wire of the cable is soldered to a female D-sub pin, and care is taken to ensure that it is not connected to the grounding shield of the cable. The other end of the cable consists of a female BNC connector. The output signal is then passed to a differential amplifier circuit mounted exterior to the test section. The circuit consists of 2 stages

of gain, both using an OP27 low noise op amp. This circuit also serves to eliminate the effects of any extraneous voltages generated between the thermocouple and the model wall. The circuit gain is 1000 to maximize signal amplitude. Due to the fact that all resistors have an inherent deviation from their intended resistance, the theoretical gain of the circuit will not be equal to the actual gain. As such it was necessary to measure the gain of each channel individually so that the correct gain number would be used when deconvolving the temperature signal. The gain of each channel was calculated by inputting a low amplitude sine wave signal whose frequency was similar to that of the changes in temperature during a shot. This frequency matching was important to ensure that there was no gain distortion at higher frequencies. Since the amplifier was set to have such a high gain it was necessary to measure each channel's stages individually in order to avoid saturation. It was assumed that there were no losses in the connections between the two amplifiers so that the total channel gain was recovered by multiplying the gains of the individual stages together. The circuit diagram can be seen in Figure 2.7a. Individual calibration of thermocouples is not necessary, since the temperature response of all common thermocouple types is well known. The NIST thermocouple reference tables were used to convert from voltage to temperature [35].

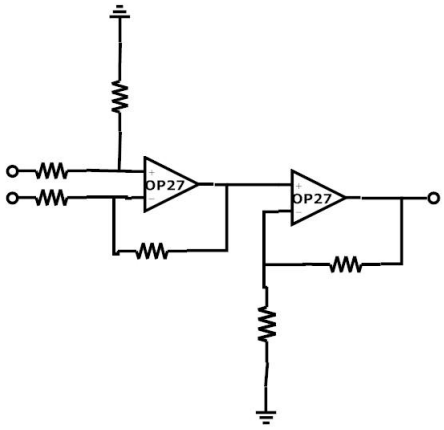

(a) Circuit diagram.

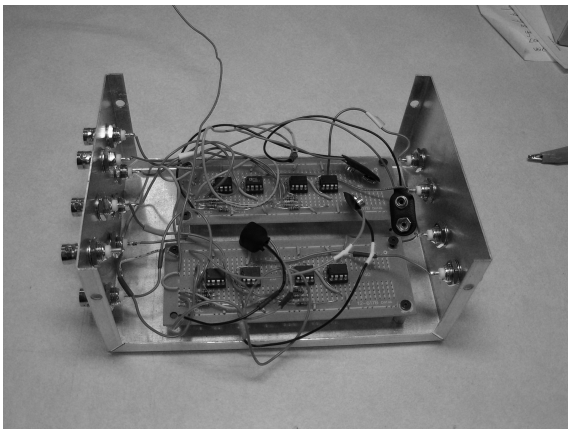

(b) Circuit box

Figure 2.7: Circuit diagram and circuit box for thermocouples.

2.2 Thin Film Gage Development

The thin film gages used in this study are based on the design of Adelgren [36], Chadwick [8], and Kinnear [37]. The gages operate based on the temperature-resistance relationship of platinum. A thin strip of platinum will have a given resistance at room temperature. As the temperature of the substrate the strip is mounted on changes, there will be a corresponding change in the resistance of the platinum strip. This response is linear, and can be determined through calibration. Since resistance is a difficult measurement to make during an experiment, the gage is used as one arm in a basic Wheatstone bridge circuit, thus converting from a temperature-resistance to a temperature-voltage relationship. The details of this circuitry will be given later in this section.

Gage construction begins by painting a thin strip of metallo-organic platinum paint on an insulating substrate, typically a form of glass or ceramic (for these experiments MACOR®was used). Henceforth the term "gage" will be defined as the insulating substrate with the thin strip of platinum painted on it. After the platinum is painted on the substrate, the gage is fired in a kiln. Multiple different firing profiles are reported in the literature for constructing the gages, and it was decided to determine a unique firing profile tailored to the furnace being used. The overall temperature settings were based on those used by Adelgren [36]. The piece was placed in the furnace and it was set to reach a maximum temperature of 642 Celsius at a ramp rate of 5 degrees per minute. This resulted in a run time of approximately 2 hours, at which point the kiln was turned off and the gage was allowed to cool overnight. This cooling period is extremely important as if the gage is removed prematurely it can result in thermal stresses causing micro-cracks in the strip of platinum paint, which can cause the gage to become non-functional. Next, this process is repeated with metallo-organic silver paint which is used to create electrical leads to the strip of platinum paint. They are fired using the same profile as the original platinum strip. At this point it should be possible to measure the resistance across the gage using the two silver leads. The gage should have a target resistance somewhere between 100 and 500 Ohms. If the gage resistance is too high, it can be lowered by painting and firing additional strips of platinum paint over the original gage. If this is done, it is important to also paint a slight layer of metallo-organic silver paint over the leads, as it is possible they will be baked away during the subsequent firings unless reinforced with more silver paint. Once the gage is within the target range wires

are attached to the silver leads using a conductive silver epoxy. Similar to the thermocouples, this wire can then be fed through the test section and into a circuit. The circuit used with these gages is a simple Wheatstone bridge circuit coupled with a single stage amplifier. The Wheatstone bridge consists of four arms, two on a left branch, and two on a right branch. The left branch arms consist of two matched, fixed resistors. These form the reference branch of the bridge. The first arm on the right branch is the thin film gage, and the second is a trimming potentiometer. The outputs of the bridge are measured after the first arms of the left and right branches. These outputs are used as inputs to a single stage differential amplifier of similar design to those used with the thermocouples. The gain of the amplifier is set to a theoretical level of 100, but it is not necessary to measure it exactly as it is taken into account during the calibration procedure. A sketch of the circuit and the actual circuit box can be seen in Figure 2.8.

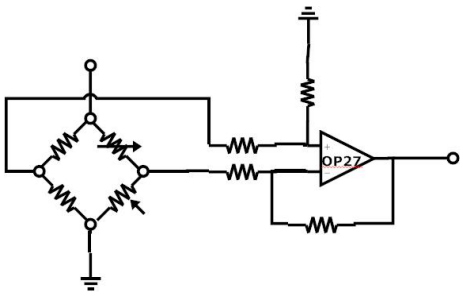

(a) Thin film circuit diagram.

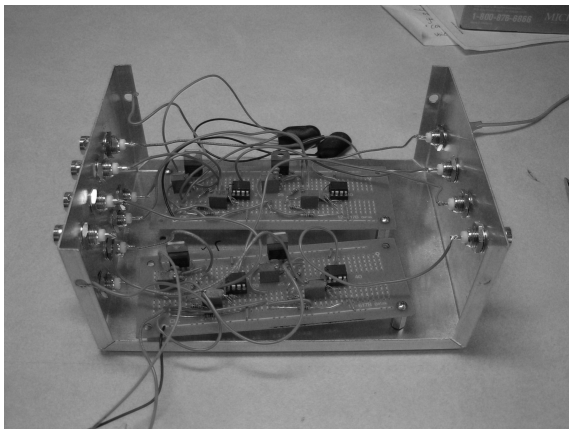

(b) Thin film circuit box

Figure 2.8: Circuit diagram and circuit box for thinfilm gages.

At the beginning of a test (when the gage is at room temperature) the trimming potentiometer is adjusted until the output of the circuit is approximately zero volts, this is known as the balanced condition. As the surface temperature(and correspondingly the resistance) of the gage changes, the bridge will be thrown out of balance and the circuit will output a voltage that is proportional to the change in resistance of the thin film gage. Since this change will be different for every gage, they must be individually calibrated. Where the sensitivity of the thermocouple gages is set solely by the type of metals used, the sensitivity of the thin film gages is highly dependent on gage geometry (including the size, shape, and thickness of the platinum strip). It is for this reason that the gage must be handled extremely carefully after it is constructed.

Even small scratches to the surface of the gage can result in a change to the gage sensitivity. As an example, when these gages were first investigated for this project they were being cleaned with a Kim wipe coated in Acetone after each calibration test. This was resulting in large changes in resistance between each calibration run, and therefore changes in sensitivity. When it was discovered that this was an issue, the practice of cleaning with a cloth and Acetone was discontinued, and there was no longer a problem with changes in gage resistance. Two different methods were investigated to calibrate the gages. The first method was suggested by Adelgren in his Ph.D. thesis [36]. During this calibration procedure, a bath of a non-conducting fluid (glycerol) is brought to a known temperature (measured with a commercial thermocouple). The bath is heated using two thermal tapes and a PID temperature controller purchased from Omega Engineering. It was found that when using the PID controller that only the proportional gain control should be used. When integral and derivative control was attempted it resulted in uncontrolled temperature oscillation in the bath. Also at issue in this setup were large thermal gradients caused by the fact that the thermal tape was mounted on the exterior of the beaker which held the glycerol. To overcome this, a basic mixer was built from a computer fan, threaded rod, and small propeller. A trim potentiometer was used to control the fan speed so that the rate of mixing could be set. Once a constant temperature has been established in the bath the gage is immersed in the liquid, the temperature in the gage substrate is allowed to equilibrate, and a voltage reading is taken. This procedure is repeated for a range of temperatures , and a calibration curve is fit to these data points. An example of one of these calibration curves is presented in Figure 2.9a. The second calibration procedure utilized a furnace instead of a glycerol bath. The gage was placed in the furnace and it was brought to a series of temperatures between 25° C and 50° C. The voltages were recorded and a calibration curve was constructed. To check the functionality of the gages, a constant heat flux source was applied to the calibrated gage. The temperature profile and resultant heat flux data are shown in Figure 2.10.

Initial experiments with the thin film gages were done with isolated gages painted on scrap pieces of MACOR®. These tests were run in order to determine the optimal firing profile, gage size, and calibration technique. Once the method of construction and testing had been developed to a satisfactory level several thin film gages were painted onto a stagnation sphere model. Also, a special insert was made which could be

mounted in a flat plate. This insert was 3 inches long and 0.5 inches wide, and was designed to have 12 thin film gages on the surface. Channels were cut in the side of the insert so that wires could be attached to each gage without affecting the surface of the model. A calibration curve for a stagnation sphere gage is shown in Figure 2.9b.

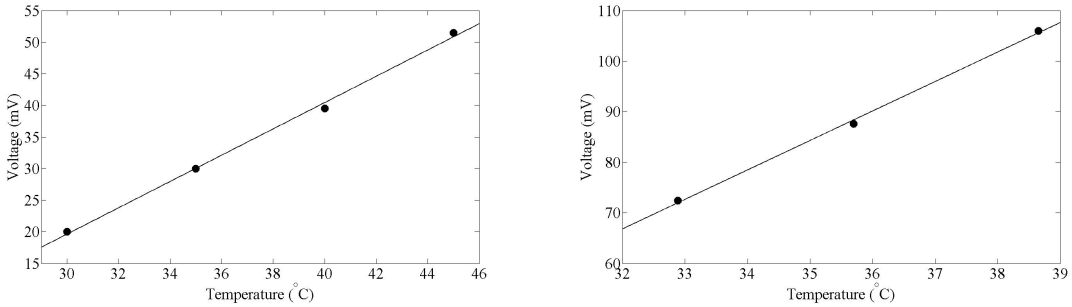

(a) Calibration of an isolated thin film gage element.

(b) Calibration of a model-mounted thin film gage.

Figure 2.9: Thin film calibration curves.

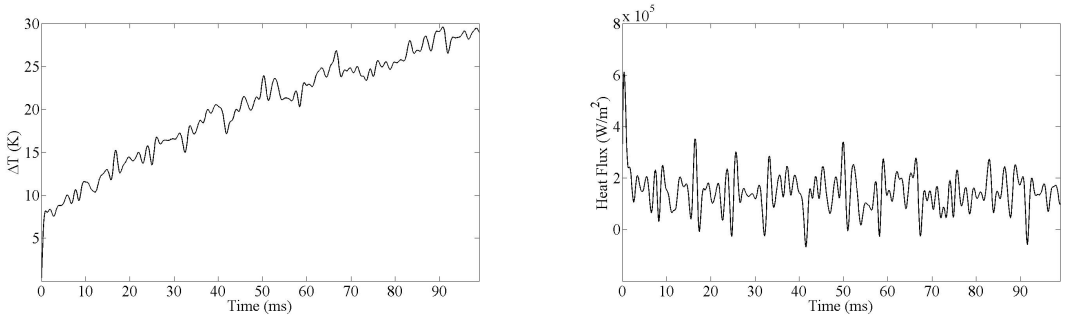

(a) Temperature history.

(b) Surface heat transfer.

Figure 2.10: Thin film gage data obtained from an isolated gage element exposed to a constant heat flux.

2.3 Heat flux deconvolution

Two methods were investigated to deconvolve the heat flux from the gages, both of which assumed that the gage or substrate can be modeled as semi-infinite body during the test time. The first method uses Laplace transforms to solve the heat equation, and this solution is shown in Equation 2.1 [38]. In order to solve this problem numerically, it is useful to use the discretized form, seen in Equation 2.2 (where the

signal consists of $n+1$ measurements).

$$\dot{q}(t) = \sqrt{\frac{\rho c k}{\pi}} \int_0^t \frac{dT(\tau)}{d\tau} \frac{d\tau}{\sqrt{t-\tau}} \tag{2.1}$$

$$\dot{q}_n = \sqrt{\frac{\rho c k}{\pi}} \sum_{i=1}^{n} \frac{T_i - T_{i-1}}{\sqrt{t_n - t_i} + \sqrt{t_n - t_{i-1}}} \tag{2.2}$$

where $\dot{q}(t)$ is the heat flux as a function of time, ρ, c, k are density, specific heat and thermal conductivity of the material respectively, and T is the temperature. The second method was introduced by Sanderson [16]. The solution to the diffusion equation in a semi-infinite plate exposed to a surface heat flux is represented by a convolution integral

$$\Delta T(x,t) = \int_0^t g(x, t-\tau)\dot{q}(\tau)d\tau \tag{2.3}$$

where ΔT is the change in temperature and $g(x,t)$ is the impulse function, given by

$$g(x,t) = \frac{\partial \Delta T(x,t)}{\partial t} = \sqrt{\frac{\alpha}{\pi k^2 t}} \exp \frac{-x^2}{4\alpha t} \tag{2.4}$$

where α is the thermal diffusivity and x is the junction depth. By taking the Fourier transform of the equation, it is possible to solve for the heat flux, such that

$$\dot{q}_n = FFT^{-1}\left[\frac{S_n}{G_n}\right] \tag{2.5}$$

where S_n and G_n are the Fourier transforms of the temperature signal and the impulse function respectively. While the signal is in the frequency domain, a low-pass, 4th order filter is applied to it. The cut-off is set to 20 kHz, as previous reports have shown that the gages carry little to no signal above this frequency range [16, 17, 18]. Comparison of the heat flux calculated using both these methods showed that the spectral deconvolution method resulted in a less noisy signal, in agreement with the results of Sanderson [16]. It should be noted that Sanderson's method of spectral deconvolution is specific to the thermocouples of his design. Thus, The numerical integration method was used with the thin film gages, and spectral deconvolution was used with the thermocouples.

2.4 Model Design

Two different model geometries were used in this work, a one inch stagnation sphere and a flat plate. As will be discussed later in this document, the stagnation sphere was originally chosen due to the fact that there is an analytical solution for the heat transfer at the stagnation point. When choosing the sphere diameter it was desirable to choose a size which would allow easy mounting of the thermocouple, and maximize the heat flux (to maximize the signal). Additionally, it was necessary that MACOR®rod was available in the diameter desired such that a thin film model could be constructed of the same size. Since stagnation point heat transfer decreases with increasing sphere radius, a one inch sphere was chosen as it was determined that any smaller would make thermocouple mounting as well as sting mounting difficult. Due to the fact that it was shot tested, the sting designed by Sharma [1] was used as the mounting base in both the thermocouple and thin film stagnation sphere designs. The thermocouple stagnation model was constructed from a one inch ball of basic carbon steel. A 0.098 inch through hole was drilled in the sphere for thermocouple mounting. A blind hold was drilled and tapped for 3/8-18 on one side of the sphere (concentric to the thermocouple hole) for mounting. The mounting rod was a 0.375 inch diameter piece of carbon steel externally tapped for 3/8-18 on both sides. This was designed to be threaded into a mounting plate which can be mounted to the sting designed by Sharma. The corresponding thin film model was made from a one inch diameter rod of MACOR®. One face of the rod was machined such that it would have a one inch diameter spherical nose radius. Two channels were cut down the sides of the rod in order to allow the wires which were connected to the gage to be fed through the mount. The rod was sleeve mounted to the same sting used for the thermocouple model. The sleeve was designed to have the same inner diameter as the rods outer diameter (allowing the rod to have a sliding fit with the sleeve). Three holes were drilled at equal spacing around the sleeve and tapped with 8-32 threads. These holes were used for set screws which were used to hold the rod in place during the shot. An additional hole was drilled in the sleeve to allow the wires to be fed through the sleeve. Also, when the MACOR rod was mounted in the sleeve a rubber stopper was inserted behind the rod. This rubber stopper was intended to be a cushion should the set screws fail during the shot so that the rod would not forcibly impact the metal sleeve mount.

For the flat plate model an entirely new mounting system was required in order to limit flow blockage

as well as allow a plate of sufficient length. To accomplish this a new sting was required which would allow models to be top mounted instead of rear mounted. The sting was designed such that it could used the same support plate as the sting designed by Sharma such that the HET would not have to be retrofitted in order to mount this sting. The height of the sting was designed with the idea that later experiments would utilize a curved ramp model. A preliminary version of this model was designed, and the necessary sting hight such that the centerline of the curved model would line up with the centerline of the tube was calculated. The new sting was also designed to have a hollow center, as well as a feedthrough hole so that wires could be fed out of the sting. When designing the flat plate, two design criteria were used. First, it had to be able to protect any wires from gages such that they would not be exposed to the flow and could be fed through the sting. Second, the model should be easily interchangeable so that different model geometries could be tested at a later date (such as the curved ramp model mentioned earlier). As such it was decided to make the plate out of three parts, a removable leading edge, the actual flat plate, and a mounting tray. The leading edge is one inch long and was made removable so that the leading edge geometry could be maintained between models to eliminate any inconsistencies between datasets from different models. It was designed to be made out of A1 tool steel in case it was decided to harden the leading edge at a later time. Mounting to the flat plate was accomplished by two 1/4-20 socket head bolts. The flat plate was designed to be 8.75 inches long and 0.25 inches thick, giving the model a total length of 9.75 inches. It was also made such that a tripping element could be mounted at 3 inches from the leading edge. The mounting tray was designed to be the interface between the flat plate and the sting. The tray is mounted to the sting using four 5/16-18 bolts. There are two mounting locations for the sting on the tray to allow visualization of both the leading edge and the rear portions of the model through the windows of the HET. The connection between the model and the tray was initially made with four 1/4-20 bolts and designed to be 0.25 inches thick. After approximately 50 shots this tray failed during a shot. The failed tray with the flat plate still installed can be seen in Figure 2.11. It was decided to redesign the tray to be much more sturdy, and as such it was re-designed to be 0.5 inches thick, and connect to the flat plate using four 3/8-18 bolts. Some of the interior volume of the tray was also machined away in order to make room for the gage wires to be fed through, and holes were drilled through the tray at both sting mounting locations to allow the wires to pass through the tray and into the sting.

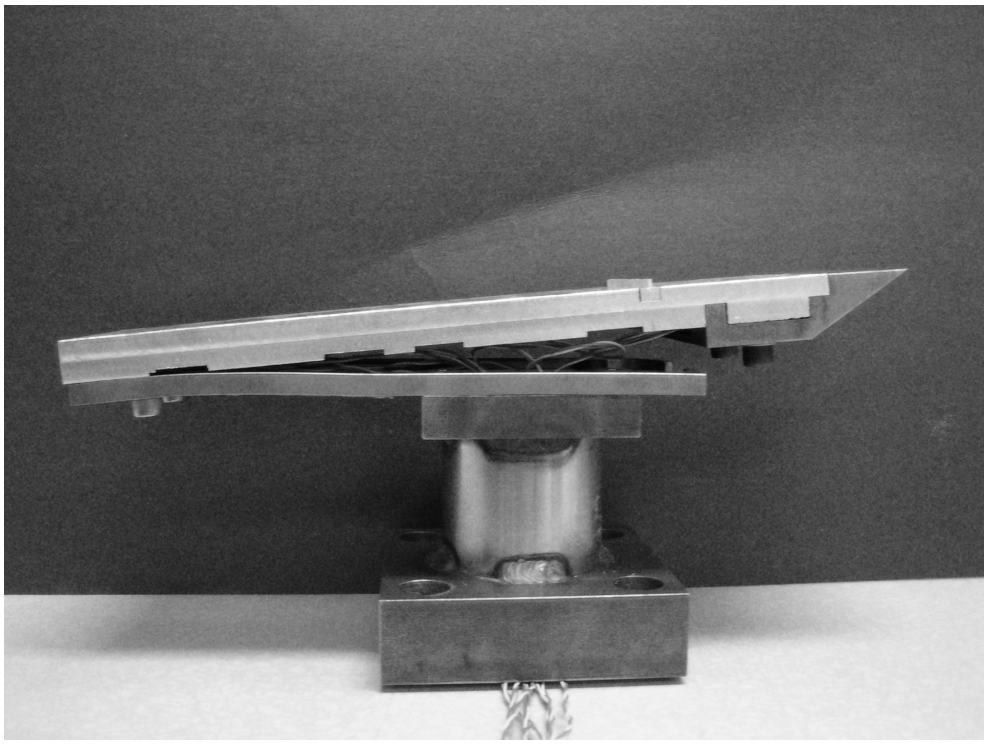

Figure 2.11: Initial tray failure

2.5 Schlieren setup

When the models were first run in the HET, Schlieren imaging was used to interrogate the flowfield around the model both to look for boundary layer growth and to check for any anomalies. The Schlieren setup was a modified z-type. The modification to the typical z-type was in the form of a third mirror which turned the light. This was necessary due to size constraints from both the room size and the size of the optical table. White light was generated using a Xenon nanopulser spark gap. This spark gap created a burst of light with a pulse width of approximately 20 ns. The system was triggered using a PCB 113A26 pressure transducer. This transducer was wall mounted in the driven section and was triggered by the initial shock. It should be noted that this is a different triggering set up to that typically used in the HET. For most shots, the Schlieren system is triggered using a 113A26 transducer mounted as a pitot probe in the test section. As such, the trigger level can be set high enough that only a very short delay is necessary, and there is very high confidence that the picture is taken during the test time. For the flat plate model used in these experiments it was impossible to mount a pitot probe inside the test section. The only other option for a shock based

triggering mechanism were the wave speed transducers mounted in the driven section. Due to the fact that these transducers are mounted significantly upstream of the test section there is much more uncertainty in the time between shock arrival at the wave speed transducer and the arrival of the test gas in the test section. When characterizing the run condition care was taken to ensure that good data was taken with both wave speed transducers and the pitot probe. This data was compared and it was found that adding a delay of 1.556 ms would put the light pulse in the middle of the test gas, and that the variations in elapsed time between the shock arrival and test gas arrival were small enough that this pulse would always be within the test gas. The light from the spark gap was collimated using a 4 inch, f10 mirror. The collimated light beam was then passed through the test section. After exiting the text section the mirror was then turned and focused using another 4 inch f10 mirror. The focused light was then turned again using a 2 inch turning mirror. Finally the light was fed past a razor blade which acts as the Schlieren cutoff. The camera used to capture the images was a pco.1600 CCD camera (Cooke Corperation) with a Nikon zoom lens attached to it. Images were recorded on a PC using the CamWare software provided by PCO. A sketch of the Schlieren set up with an example light beam going through the test section can be seen in Figure 2.12.

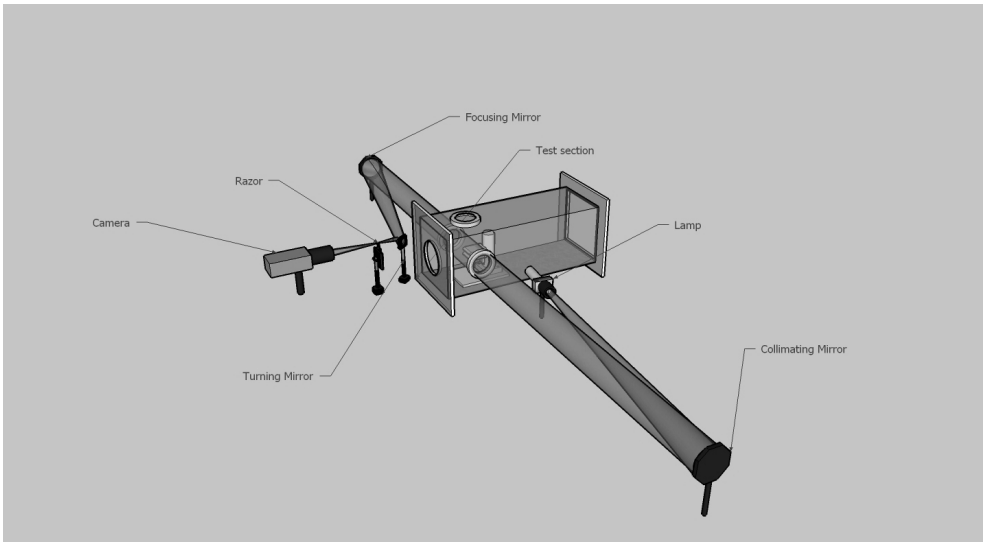

Figure 2.12: Sketch of Schlieren set up.

Chapter 3

Results

Two canonical model geometries were investigated in this study, a stagnation sphere and a flat plate. These models were chose both for their simplicity and for the fact that theoretical predictions exist for both model types.

3.1 Theoretical Predictions

The task of predicting the heat transfer at the stagnation point in high speed flows was first undertaken by Fay and Riddell [39]. By treating air as a binary mixture of molecules and atoms and limiting themselves to the stagnation point they showed that the boundary layer equations can be reduced to a set of self-similar equations, even when accounting for arbitrary chemical reaction rates. This result allowed them to find numerical solutions for the stagnation point heating even when the boundary layer was not in a frozen or equilibrium condition. Additionally, they were able to run a parametric study using their numerical solution over a wide range of altitudes and flight speeds when assuming either an equilibrium or frozen boundary layer. They were able to perform curve fits to this data and develop analytical solutions for the heat flux for both the frozen and the equilibrium boundary layer. One more variable that was taken into account in the study was the effect of wall catalysis. For the case of the equilibrium boundary layer wall catalysis is a non-issue as it is not possible for any further chemical reactions to occur at the wall. Alternatively, when the flow is frozen, wall catalysis can have a significant effect on the stagnation point heat transfer. When developing their equations, Fay and Riddell considered two different wall catalysis conditions, non-catalytic and fully catalytic. In the non-catalytic case there are no reactions at the wall, and the flow maintains the same concentration of molecules and atoms as it did throughout the boundary layer. The fully catalytic

condition indicates that there is full recombination at the wall, and therefore the fluid at the stagnation point consists only of molecules. It is important to note that in all these calculations, the gas was air, and therefore they are not valid for other gases.

Equilibrium boundary layer:

$$q = 0.94(\rho_w \mu_w)^{0.1}(\rho_s \mu_s)^{0.4} \times \left\{1 + (Le^{0.52} - 1)(h_D/h_s)\right\}(h_s - h_w)\sqrt{(du_e/dx)_s} \tag{3.1}$$

Frozen boundary layer, non-catalytic wall:

$$q = 0.94(\rho_w \mu_w)^{0.1}(\rho_s \mu_s)^{0.4} \times \left\{1 - (h_D/h_s)\right\}(h_s - h_w)\sqrt{(du_e/dx)_s} \tag{3.2}$$

Frozen boundary layer, fully catalytic wall:

$$q = 0.94(\rho_w \mu_w)^{0.1}(\rho_s \mu_s)^{0.4} \times \left\{1 + (Le^{0.63} - 1)(h_D/h_s)\right\}(h_s - h_w)\sqrt{(du_e/dx)_s} \tag{3.3}$$

There has been some work performed after the development of these equations to simplify them so that they may be applied more easily, and to extend them to different gases. Sutton and Graves [40] developed an equation for the equilibrium boundary layer that can be used to calculate the stagnation point heat flux for an arbitrary test gas. Their equation is given in Equation 3.4.

$$\dot{q} = K\sqrt{\frac{p_s}{R}}\,(h_{0,e} - h_w) \tag{3.4}$$

Where K is a constant based on the gas composition. Another expression was computed by Filippis in order to extend the predictive range of the theory from a maximum flow enthalpy of 23 MJ/kg to 39 MJ/kg [41]. This is shown in Equation 3.5.

$$\dot{q} = 90\sqrt{\frac{p_s}{R}}\,(h_{0,e} - h_w)^{1.17} \tag{3.5}$$

Though the experiments done here are within the 23 MJ/kg limit, the two equations still yield different results, and thus the experimental measurements were compared against both theoretical predictions.

Theoretical predictions for laminar flat plate heat transfer were calculated with the reference enthalpy

method of Simeonides [42], shown in Equation 3.6.

$$\frac{\dot{q}_w L P^{2/3}}{\mu_e c_p \left(T_{rec} - T_w\right)} = C \left(\frac{p_e}{p_e}\right)^{(1-n)} \left(\frac{T_e}{T^*}\right)^{(1-n)} \left(\frac{\mu^*}{\mu_e}\right)^n \left(\frac{u_{main}}{u_e}\right)^{(1-2n)} \left(u_{grad}\frac{L}{u_e}\right)^n \mathrm{Re}_{e,L}^{(1-n)} \quad (3.6)$$

and predictions of turbulent flat plate heat transfer were made using the Van Driest II method [43], an explanation of which can be found in Sharma's thesis [1].

3.2 Stagnation point results

To obtain directly comparable experimental results for both gages, two spherical models were designed. A thermocouple is mounted at the stagnation point of a 25.4 mm diameter stainless steel sphere, Figure 3.1; this model can be seen sting-mounted in the test section of the HET in Figure 3.2. For the thin film gages, a hemispherical blunt-body model with 25.4 mm nose diameter was created from the gage substrate material (in this case machinable ceramic MACOR®), then sleeve-mounted to the sting. Three gages were painted in the stagnation region, one at the stagnation point and two slightly offset. The MACOR thin film substrate model is shown in Figure 3.3.

Figure 3.1: Thermocouple mounted at the stagnation region of a 25.4 mm diameter sphere model.

Thermocouple data were taken at three different test conditions with calculated stagnation enthalpies from 4.09 to 7.52 MJ/kg (listed in Table 2.2). Figures 3.4, 3.5, and 3.6 show the comparison between the

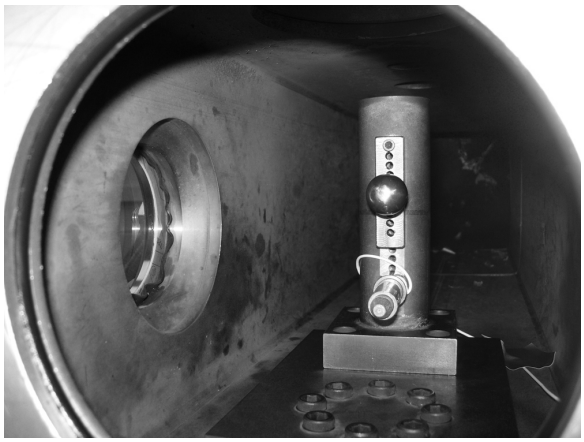

Figure 3.2: Thermocouple stagnation sphere mounted in HET test section.

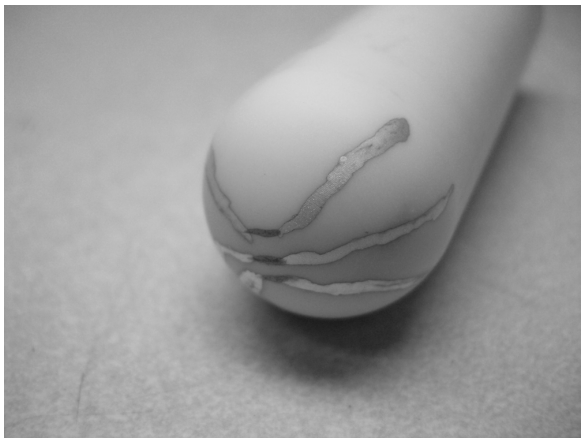

Figure 3.3: Three thin film gages painted on the stagnation region of a 25.4 mm diameter MACOR®substrate model.

temperature rise and the pitot pressure trace over a time period which encompasses the test gas. In all three plots, the temperature trace shows the arrival of the initial shock, accelerator gas, and contact surface, and the response time compares very well with the pitot pressure histories. The response time of the thermocouple gage was found to be sensitive to the degree of sanding used to create the thin thermocouple junction.

The experimentally measured heat fluxes for each condition, and the theoretical predictions are listed in Table 3.1. It is evident that in every case the heat transfer is under-predicted by theory. This is consistent with the results obtained by Marineau and Hornung while calibrating a new conical nozzle in the T5 facility [44]. The equation developed by Filippis provides the best prediction of the heat flux, with a 23% deviation in Air-4, a 26% deviation in Air-5, and a 35% deviation in Air-6.

For the thin film gages, initial data was taken with the HET operating as a shock tube. The stagnation

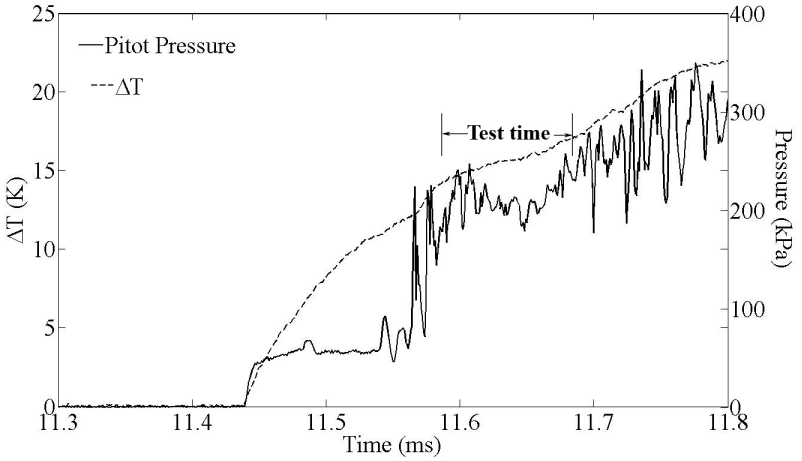

Figure 3.4: Air-4 temperature rise vs. pitot pressure.

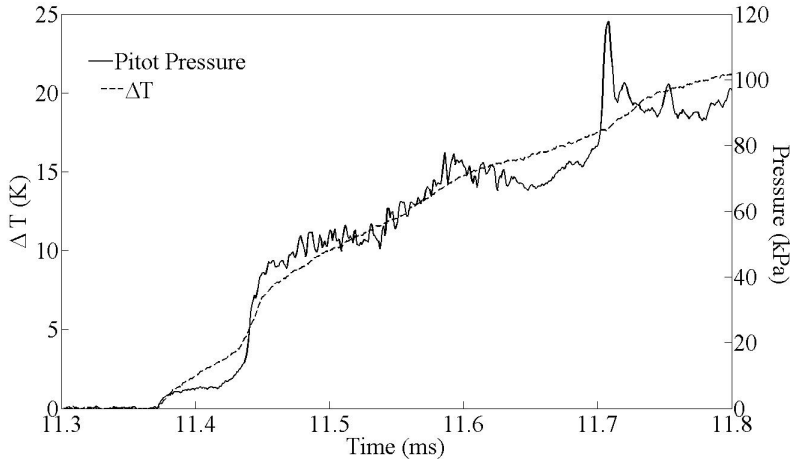

Figure 3.5: Air-5 temperature rise vs. pitot pressure.

region gage was able to capture the initial shock and subsequent temperature rise very well. The temperature trace is shown in Figure 3.7 and calculated heat transfer data is shown in Figure 3.8. Shock arrival can be seen at 11.31 ms, referenced from the primary diaphragm rupture. The temperature history is presented unfiltered. Low-pass filtered data was used for the subsequent heat transfer calculation. The average heat flux over the steady state temperature rise is 2.95 MJ/m^2.

Thin film gage survival at the stagnation point was zero under expansion tube conditions. When measured between successive shots, changes in resistance were typically on the order of 500%. This is most likely due to gage damage from the high temperatures, shear forces, and debris that the model is exposed to during an experiment. This large resistance change calls into question the accuracy of any calibration curve

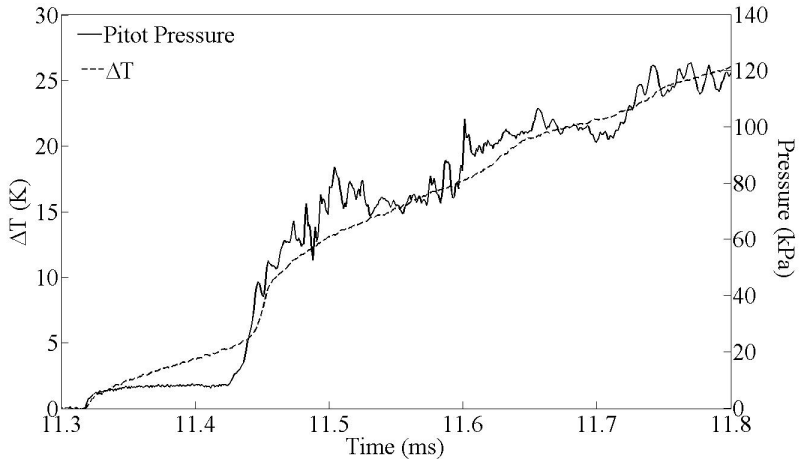

Figure 3.6: Air-6 temperature rise vs. pitot pressure.

Table 3.1: Comparison of experimental heat transfer with theoretical predictions.

	Experimental heat flux	Sutton and Graves	Filippis
Air-4	7.85±0.63 MW/m^2	6.29 MW/m^2	6.40 MW/m^2
Air-5	7.74±0.62 MW/m^2	5.41 MW/m^2	6.15 MW/m^2
Air-6	8.50±0.68 MW/m^2	5.66 MW/m^2	6.28 MW/m^2

for the gage. Since it is not known at what point in the experiment the gage was damaged, it is impossible to say if the calibration curve was still accurate during the test time. A second problem arose due to the exposed connection between the silver leads and the wire connection. Since this connection was exposed to the flow it had significant effects on the signal-to-noise ratio, decreasing confidence in the measurements.

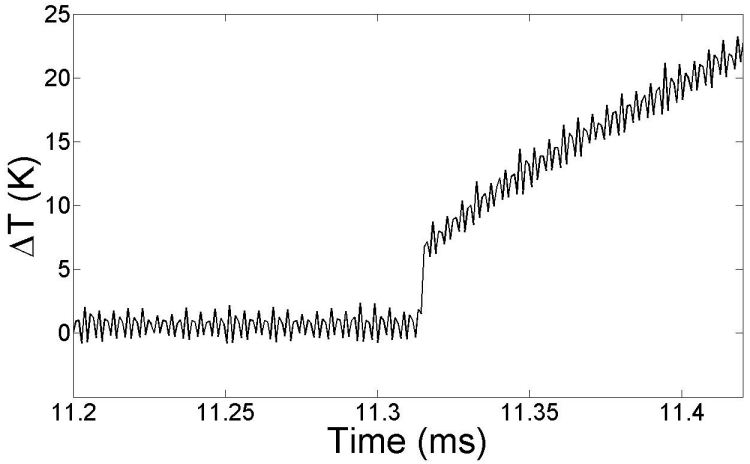

Figure 3.7: Thin film raw temperature history.

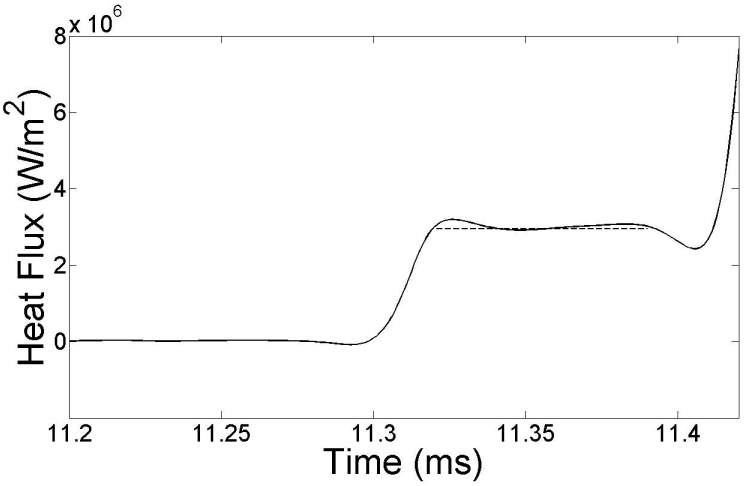

Figure 3.8: Thin film surface heat transfer.

3.3 Flat plate results

A flat plate was chosen as the second model geometry due to both its simplicity and the existence of theoretical predictions of heat flux. Also, the flat plate solved both issues discussed in Section 3.2 that were experienced with the stagnation point thin film gage. With the flat plate design the connection between the silver leads and the feedthrough wire were shielded from the flow, and the parallel mounting direction of the gages decreased the chances of damage from high temperatures and particulates in the flow. Figure 3.9 shows both the thermocouple and thin film flat plate models. These models were designed such that the same leading edge could be utilized for both the thin film and the thermocouple gages. Figures 3.10, and 3.11 show the comparison of the thin film data to the thermocouple data for the Air-4 and Air-6 run conditions, we were unable to collect flat plate data for the Air-5 condition. Both conditions show good agreement between gages near the leading edge, and measurements are in good agreement with theoretical predictions. It should be noted that both the thermocouples and thin film gages show an increase over the theory with increasing x-location on the plate. Initially this increase was more pronounced, but it was determined that we needed to account for flow establishment time, which is discussed in the next section. Even after the data was re-analyzed with the flow establishment time taken into account this rise of theory was still observed.One possible explanation may be that it is due to the beginnings of transition on the plate. This is unlikely due to the low unit Reynolds numbers of both the Air-4 and Air-6 conditions. A more likely

explanation is that there is some mechanism affecting heat flux in the experimental flow which is not taken into account in the reference enthalpy method used to make the predictions.

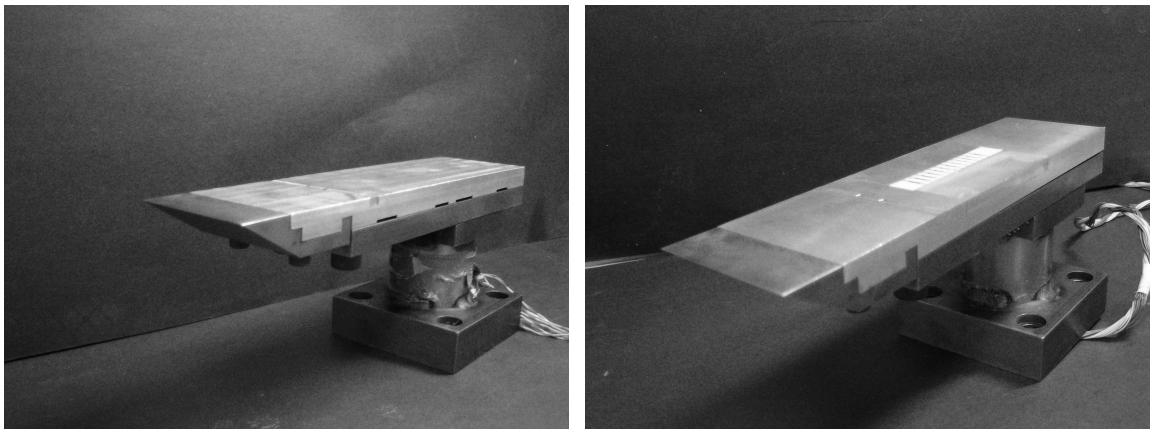

(a) Thermocouple flat plate model.

(b) Thin film flat plate model.

Figure 3.9: Flat plate models.

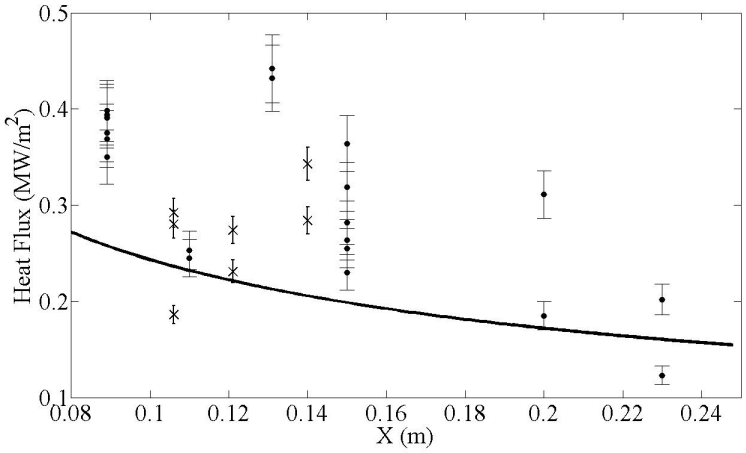

Figure 3.10: Comparison of thin film (×) and thermocouple (●) heat flux data in Air-4 (leading edge at x=0).

3.4 Unsteady Results

In the initiation of any flow over a model, there is a finite time over which the flow must establish itself over the surface of the model. During this establishment time, the flow is denoted as “unsteady” and this may have noticeable effects on the properties at the surface of the plate (including the heat transfer). The relaxation of a flow to a steady state happens in two different regimes, the external, inviscid region, and the viscous, boundary layer region. The inviscid region relaxes to steadiness quickly, within one flow length of

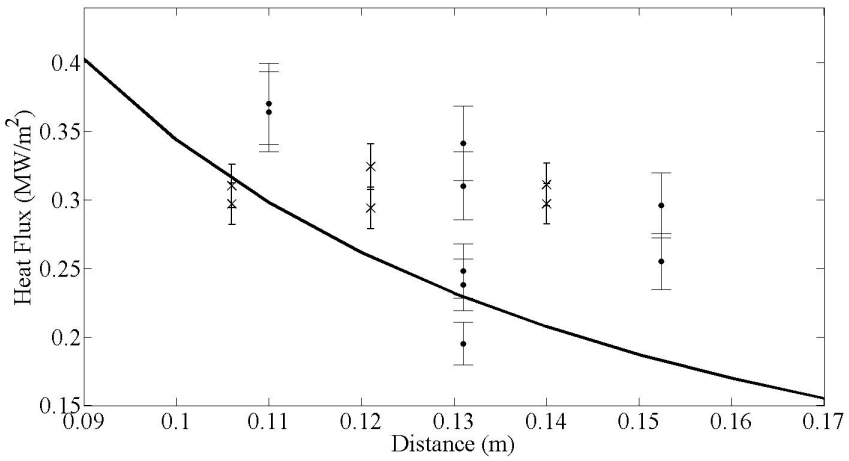

Figure 3.11: Comparison of thin film ($\times$) and thermocouple ($\bullet$) heat flux data in Air-6 (leading edge at x=0).

the model. The boundary layer relaxes more slowly due to the viscous processes which dominate the flow in this region [45]. In a recent study by Marineau, et al. [46] in the T5 facility at Caltech, it was found that at their high enthalpy condition a steady state was not achieved over the model. The result of this was that the heat flux measured in these unsteady cases was higher than theory. The prompted an investigation into unsteadiness in the HET as a possible explanation for the increase over theory that is observed in the flat plate data. Gupta [45] performed an analysis on the time required for the boundary layer to relax to steadiness on a flat plate in an expansion tube. Two different modes of expansion tube operation were identified, the Mirels limit and the Blasius limit. In the Mirels limit, the transmitted shock from the rupture of the secondary diaphragm and the contact surface are so close together that the time between their arrivals goes to zero. In the Blasius limit the transmitted shock and the contact surface are sufficiently far apart that the time between them can be said to go to infinity. In all three run conditions used here it is reasonable to assume we are in the Blasius limit. In this regime, a Blasius boundary layer is established over the flat plate during the time in which the accelerator gas is passing over it. With the arrival of the contact surface, this boundary layer is washed away, and a new boundary layer consisting of test gas must be formed. During this transition, there is a finite amount of time when the boundary layer will consist of both accelerator and test gas while it is simultaneously relaxing to a steady state. Gupta performed a series of numerical calculations and determined that there was a critical value for the non-dimensional parameter α after which steady boundary layer flow would be established in the test gas. The non-dimensional parameter is defined as:

$$\alpha = \frac{L}{u_e t} \tag{3.7}$$

Where t is the time coordinate beginning with the arrival of the contact surface. Gupta determined that at a value of $\alpha = 0.3$ the boundary layer would have relaxed to a state where it is completely composed of test gas and is steady. Since the external flow velocity of the run conditions is known, it is possible to compute the time to reach steadiness at each thermocouple location along the plate. A plot of the boundary layer establishment time at all the thermocouple locations along the flat plate can be seen in Figure 3.12.

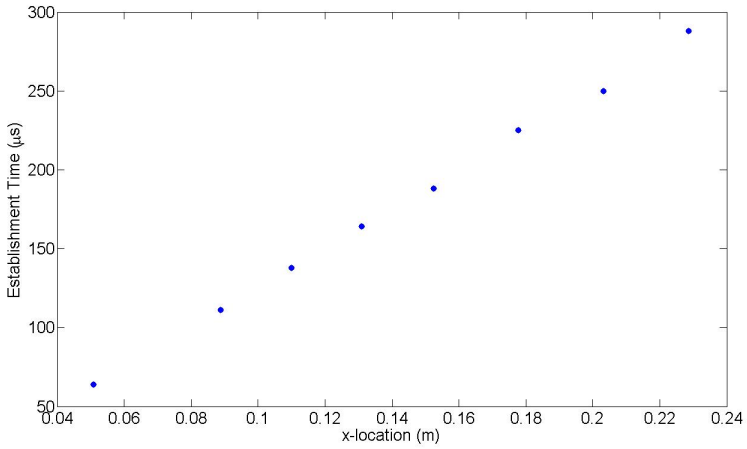

Figure 3.12: Air-4 establishment times.

The recast data plotted against the original data can be seen in Figure 3.13.

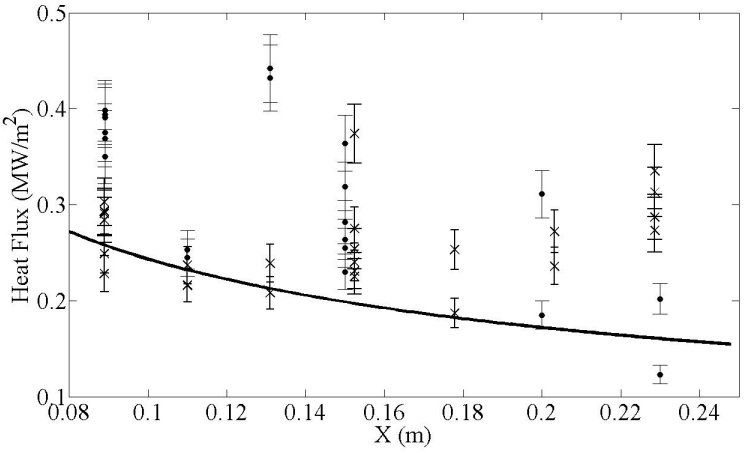

Figure 3.13: Comparison of re-cast data (•) with original analysis (×).

3.5 Schlieren Imaging

In addition to heat transfer data, schlieren images were taken over both the flat plate and sphere models. The flat plate schlieren was used to calculate the boundary layer thickness along the plate and compare it to theoretical predictions. Figure 3.15 shows the comparison of the theoretical boundary layer growth versus that measured from the schlieren images. The theoretical prediction was calculated using the method of Mallinson, et al [47], and their result is shown in Equation 3.8. The experimentally measured boundary layer is greater than theory in all cases. The reason for this deviation is not yet understood, though it could be due to measurement error. Boundary layer thickness was calculated by measuring the thickness of the white line using Photoshop editing software. The decision to use this white line as the indicator of boundary layer thickness was based on previous works [48, 49]. In a hypersonic boundary layer the maximum density gradient is in portion of the boundary layer closest to the freestream. This maximum density gradient will be represented by either an exremely light or dark line (depending on knife blade orientation) and therefore, the termination of this line can be considered to be the edge of the boundary layer. Since it is difficult to pick out the exact termination of this line with the naked eye, it could result in a bias in the data. Schlieren imaging was also used to image the bow shock for the stagnation sphere. A typical image is shown in Figure 3.16.

$$\frac{\delta}{L}\sqrt{\mathrm{Re}_L} = 1.721\left\{2.397 + \frac{T_w}{T_e} + 0.0965\sqrt{P}\,(\gamma - 1)\,M_e^2\right\} \tag{3.8}$$

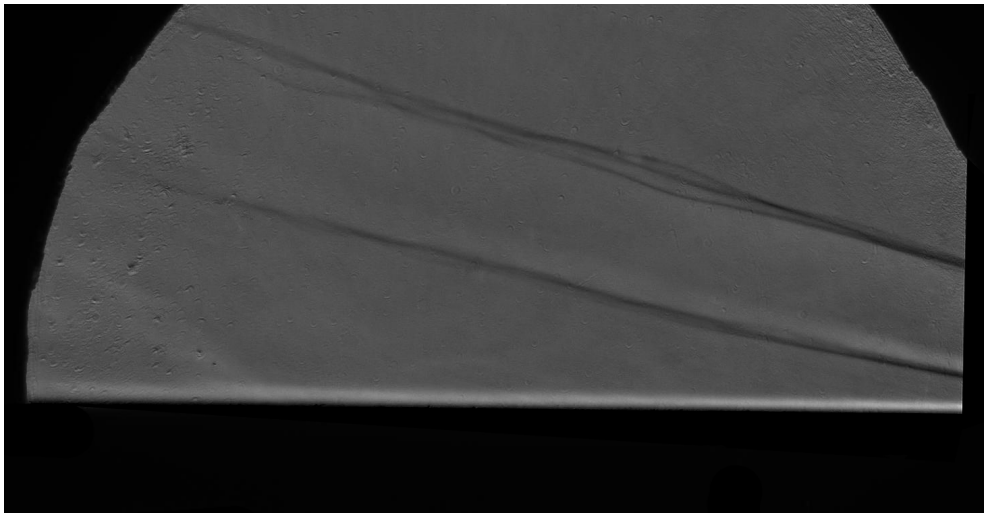

Figure 3.14: Schlieren image of the flat plate in Air-4

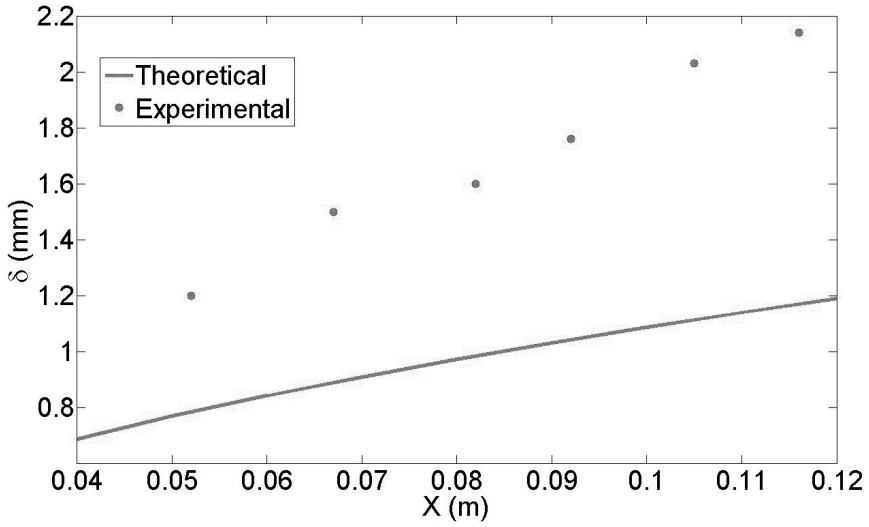

Figure 3.15: Comparison of theoretical to experimental boundary layer thickness

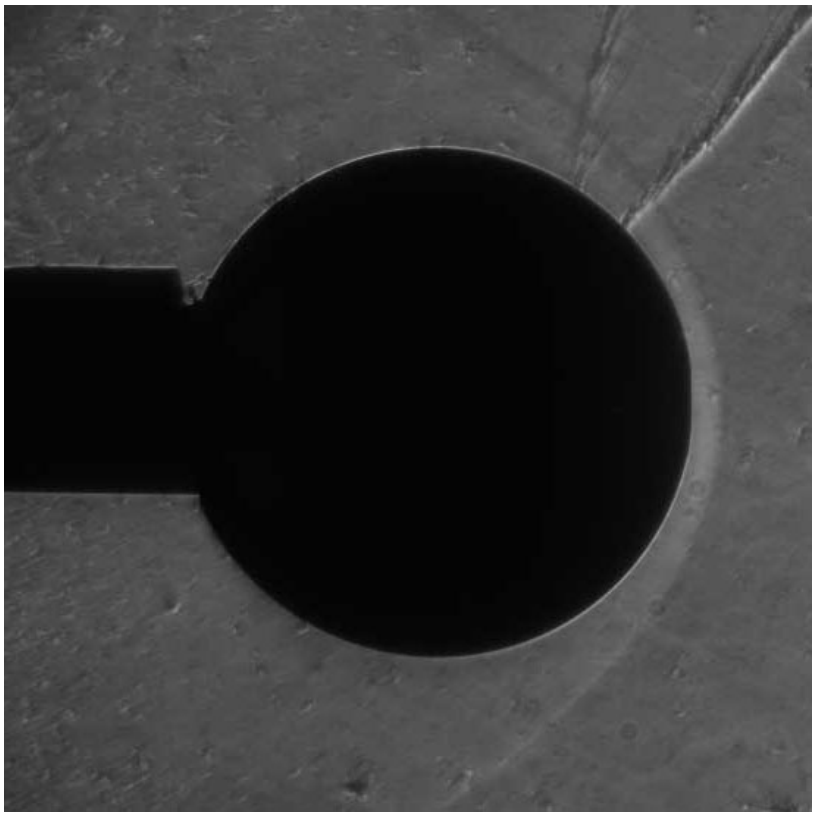

Figure 3.16: Schlieren image of the sphere in Air-4

Chapter 4

Conclusion and Future Work

Thermocouples and thin film gages are used extensively for surface heat transfer measurements in hypersonic impulse facilities. Coaxial thermocouples are robust, can survive challenging experimental conditions, and are typically used in higher enthalpy flows. Thin film resistance gages provide improved signal levels, but have to be individually calibrated, are less robust, and are typically used in lower enthalpy flows. The goal of this work is to make directly comparative measurements in flow fields accessible to both gage types with stagnation enthalpies between 4.08 and 7.52 MJ/kg.

I report on the design and construction of both coaxial thermocouples and thin film resistance thermometers. Gages are mounted on equivalent spherical and flat plate models. Thermocouple gages are internally mounted, while thin film gages are directly painted and fired onto a MACOR model which acts as the gage substrate, and calibrated in situ.

Both gages have been successfully used in the HET. Tests demonstrate that thermocouple gages are preferable for use in stagnation regions due to the extremely poor survivability of thin film gages. Both gages show good agreement in the flat plate case, though thin film gages have less noise, a higher signal level, and more consistent response time. Thus, in mounting locations where survivability is not an issue, thin film gages are the preferred gage type.

Multiple studies are planned or have already begun utilizing these gages. The direct extension of this work is investigation of heat transfer over convex curved surfaces. Multiple models have been instrumented with thermocouple gages. At this time plans include models with two different levels of curvature. Comparisons will be made to the flat plate data presented in this report in order to determine the effect on surface curvature on heat transfer. A second project utilizing these gages is an investigation into the Mars Science Lander (MSL) which is currently being undertaken. This project seeks to compare both shock

shape, standoff distance, and surface heat transfer over the MSL to CFD simulations. Though these are the only studies currently underway, the application of these gages is only limited by the geometries which are mountable in the tube itself. Future work involving shock-boundary layer interaction, and comparison to laser based diagnostics (such as PLIF) has been discussed.

The development and application of heat transfer gages in the HET is a promising step forward in the maturation of the facility. When combined with the diagnostics already implemented in the HET (including schlieren, emission spectroscopy, and pitot pressure measurements), the facility is quickly approaching the ability to fully characterize new run conditions, but also to interrogate novel model geometries with a number of different diagnostics.

Appendix A

Sting Drawings

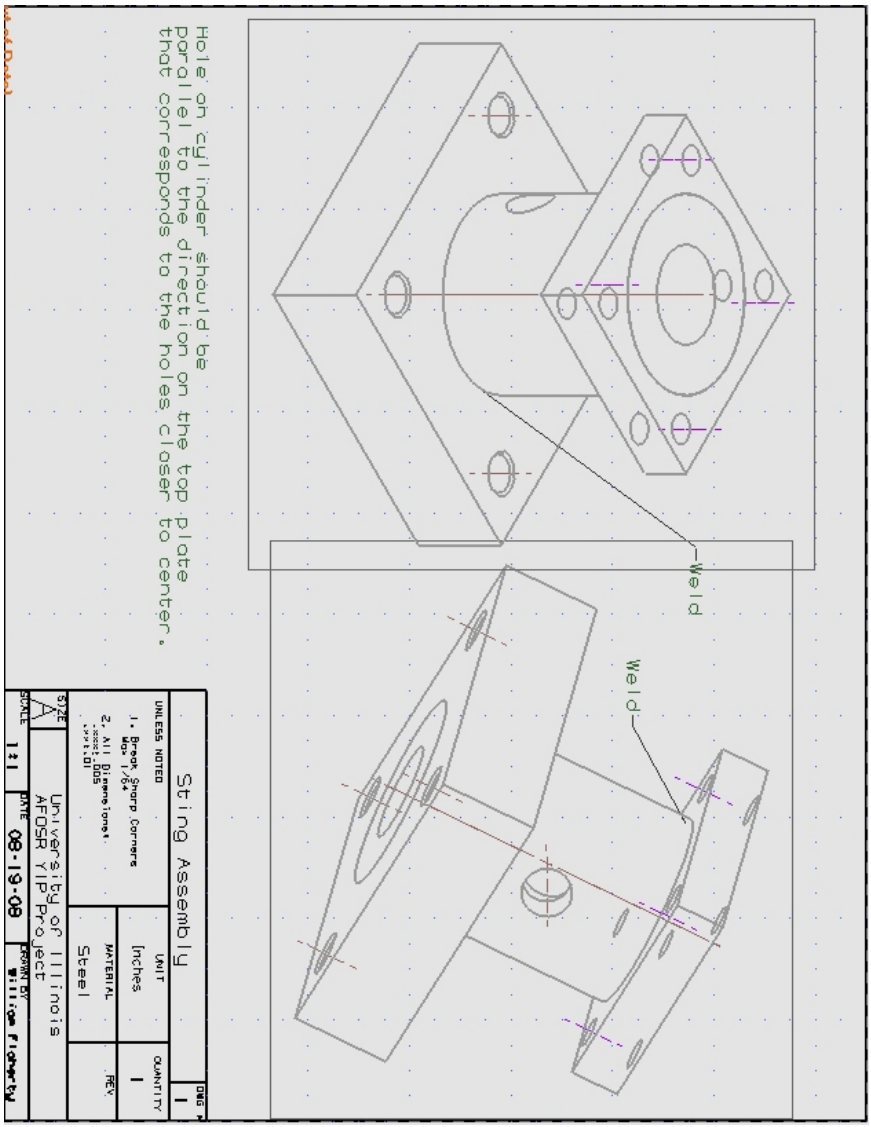

Figure A.1: Full Sting Assembly

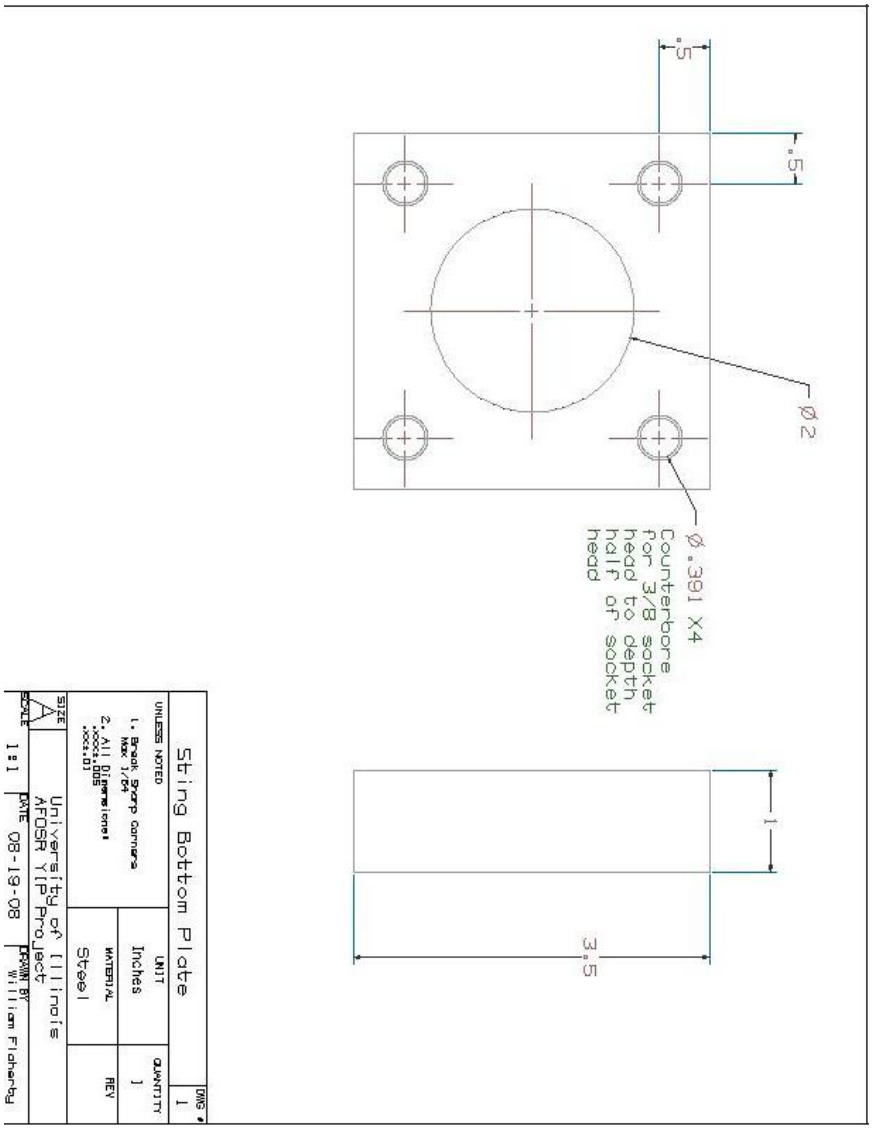

Figure A.2: Sting Bottom

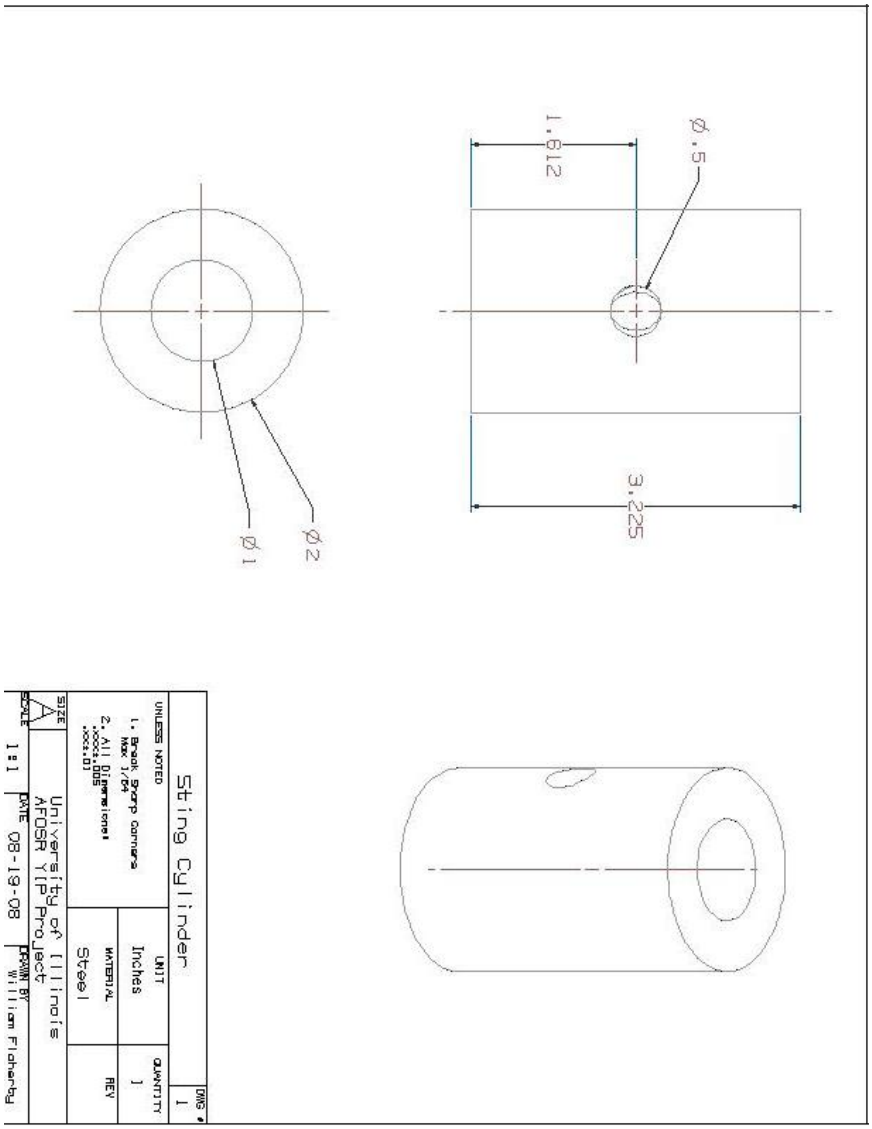

Figure A.3: Sting Cylinder

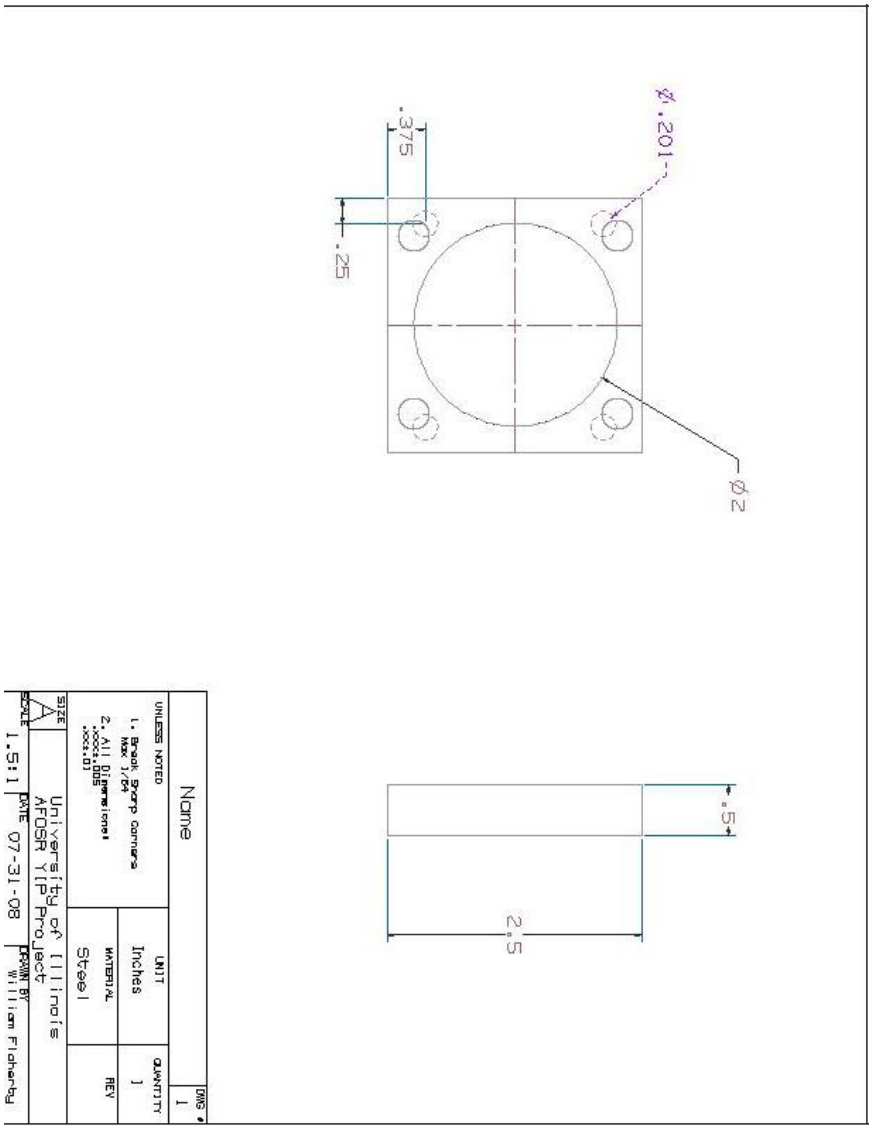

Figure A.4: Sting Top

Appendix B

Thermocouple Flat Plate Drawings

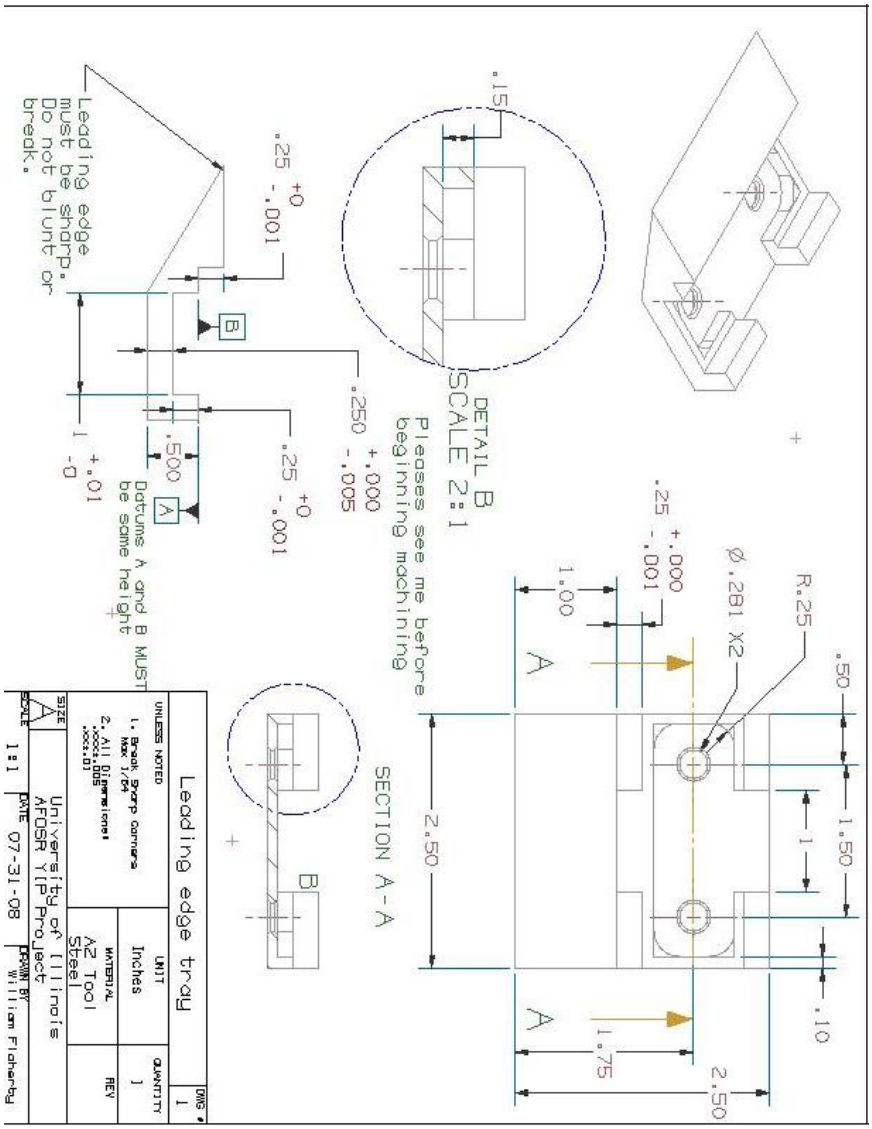

Figure B.1: Leading Edge

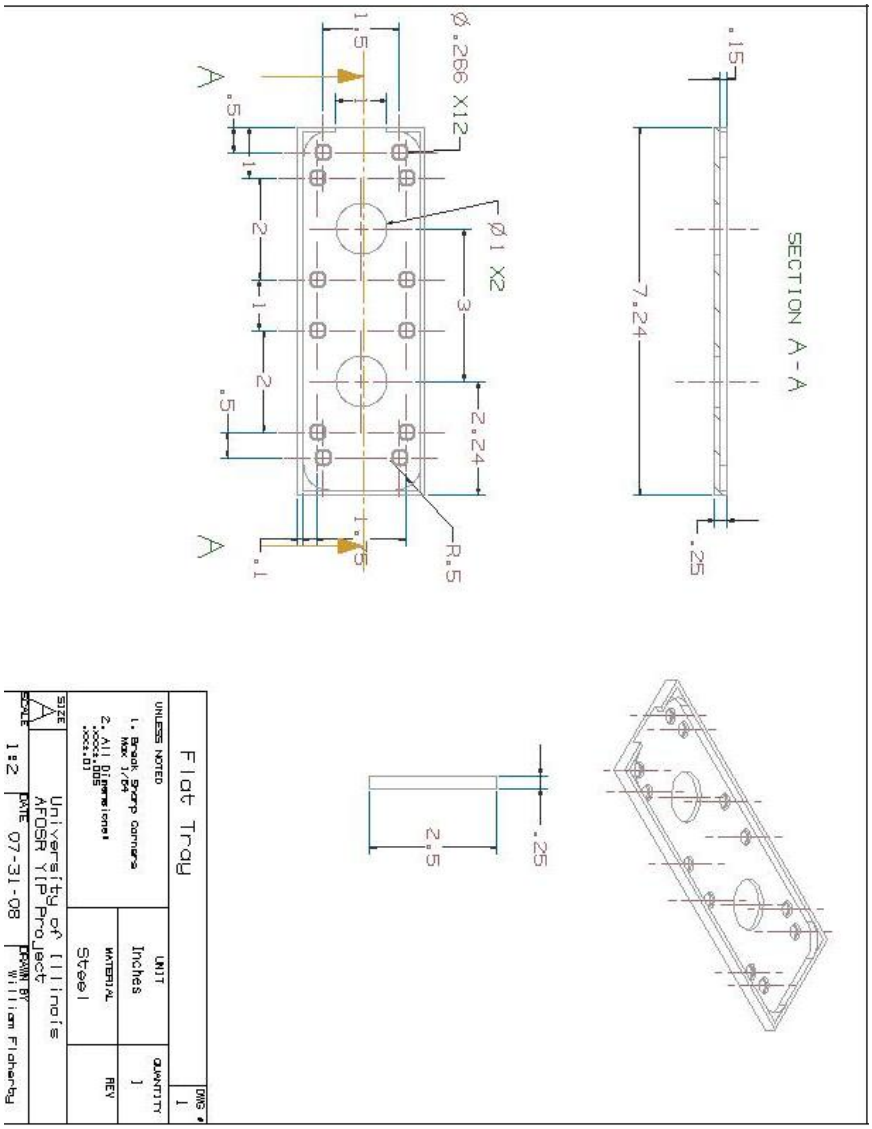

Figure B.2: Original Tray

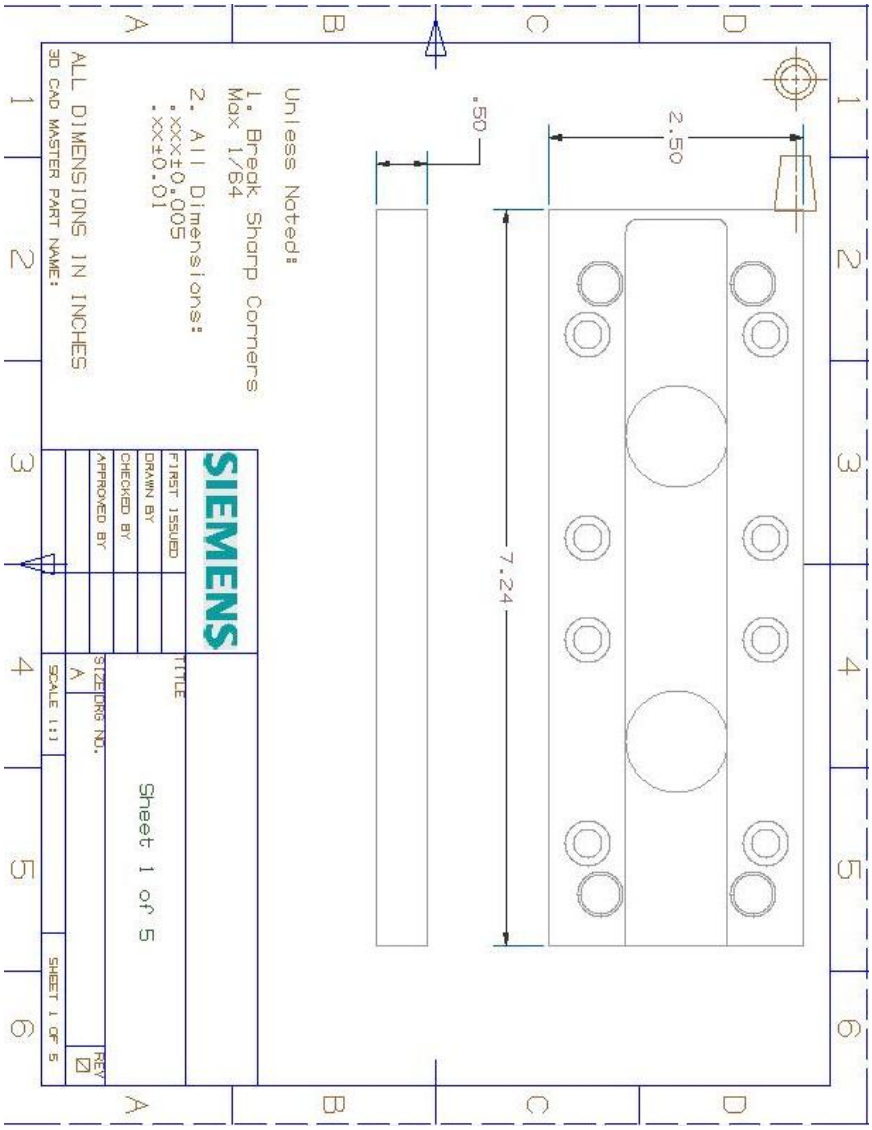

Figure B.3: Thick Tray

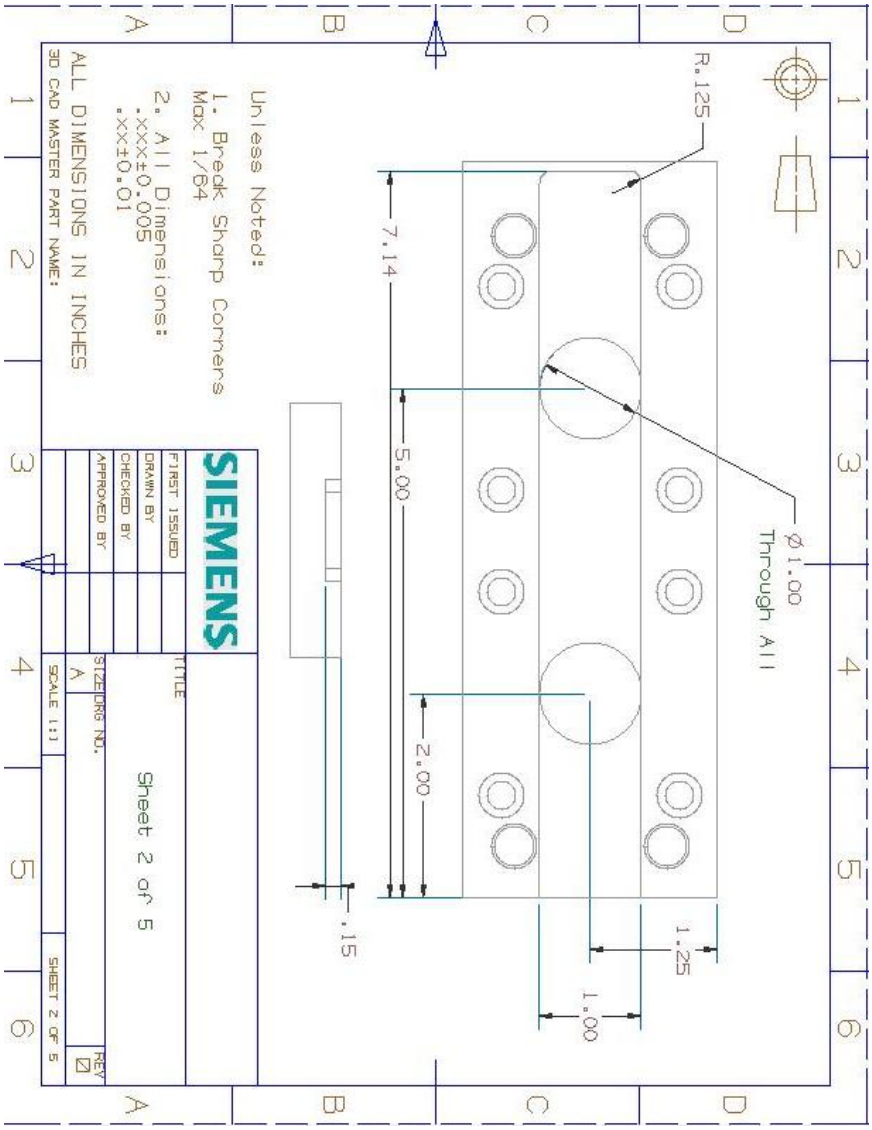

Figure B.4: Thick Tray

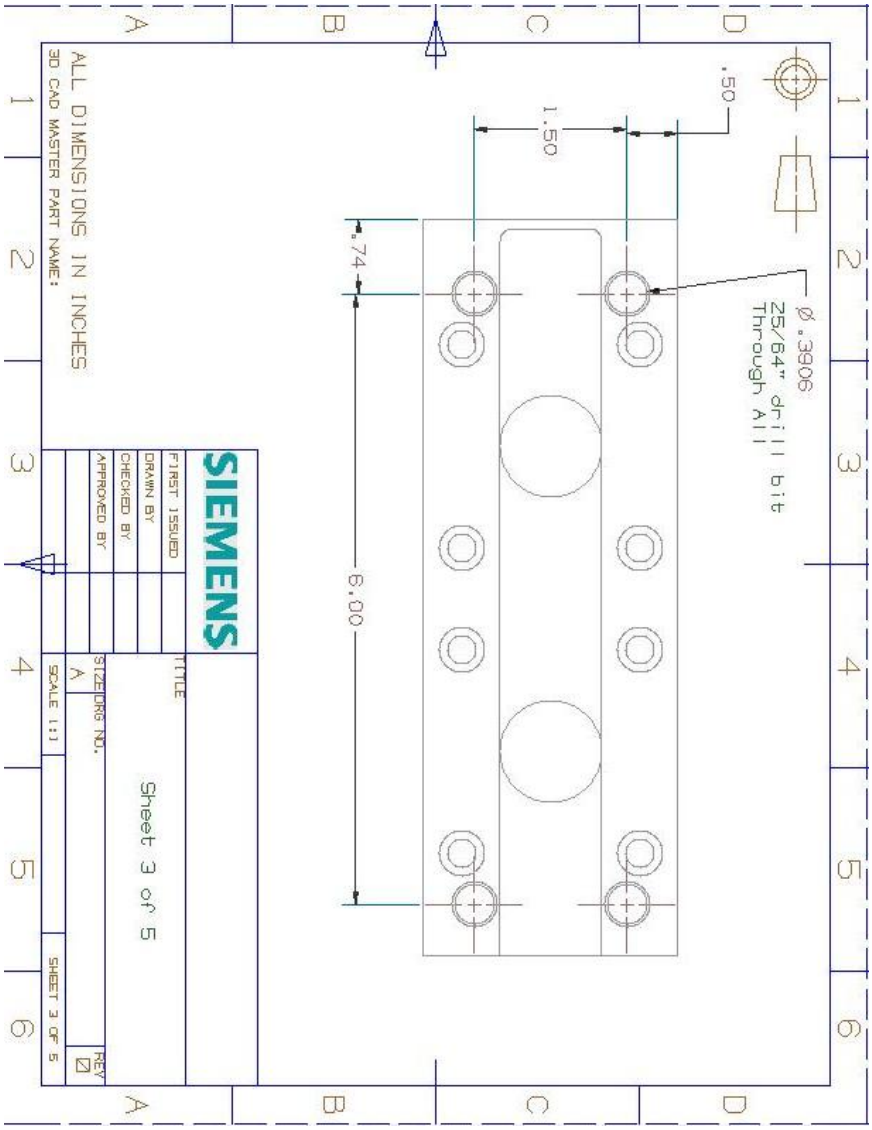

Figure B.5: Thick Tray

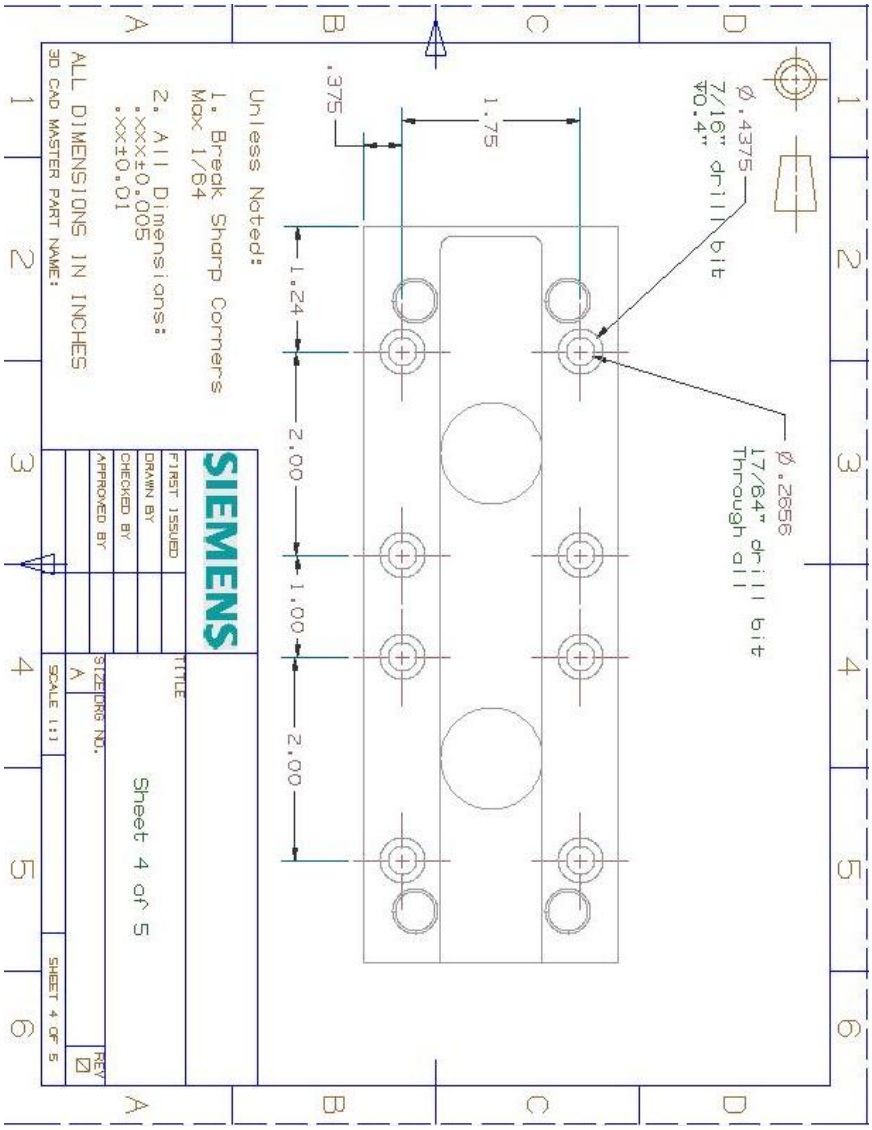

Figure B.6: Thick Tray

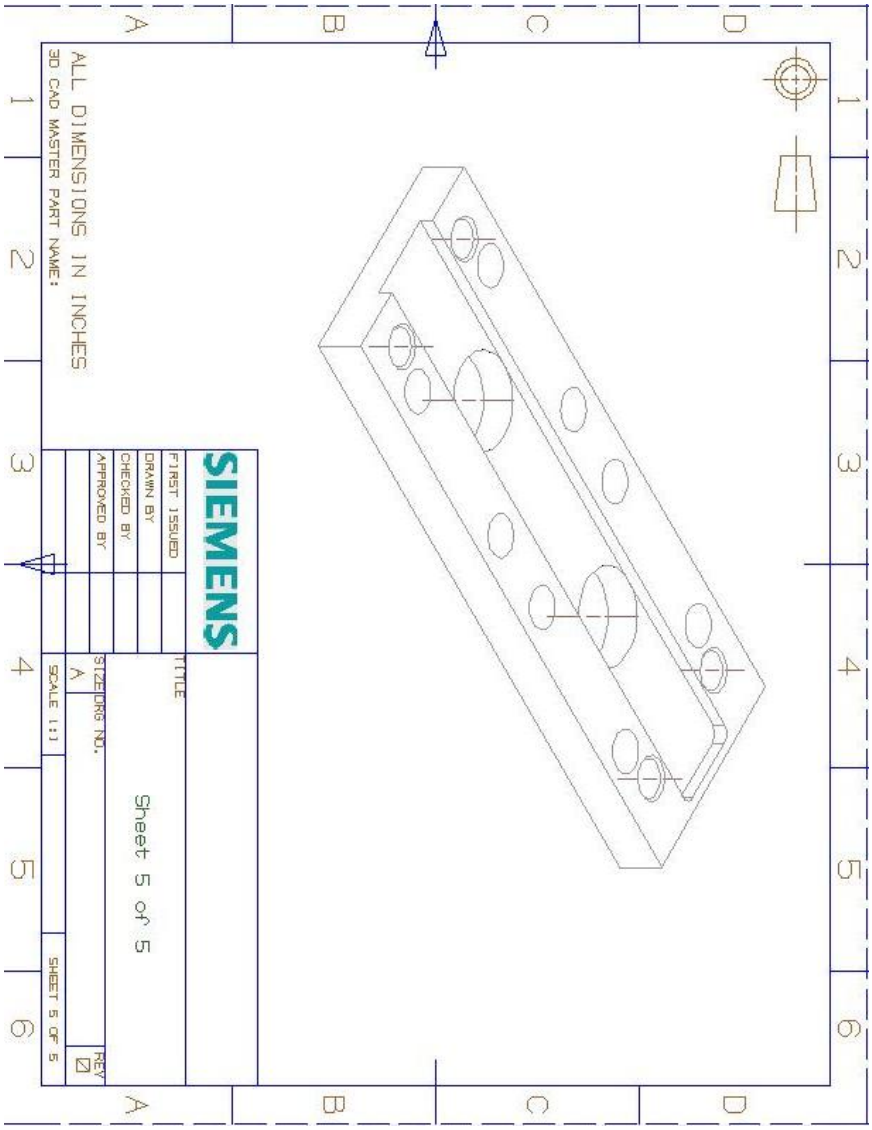

Figure B.7: Thick Tray

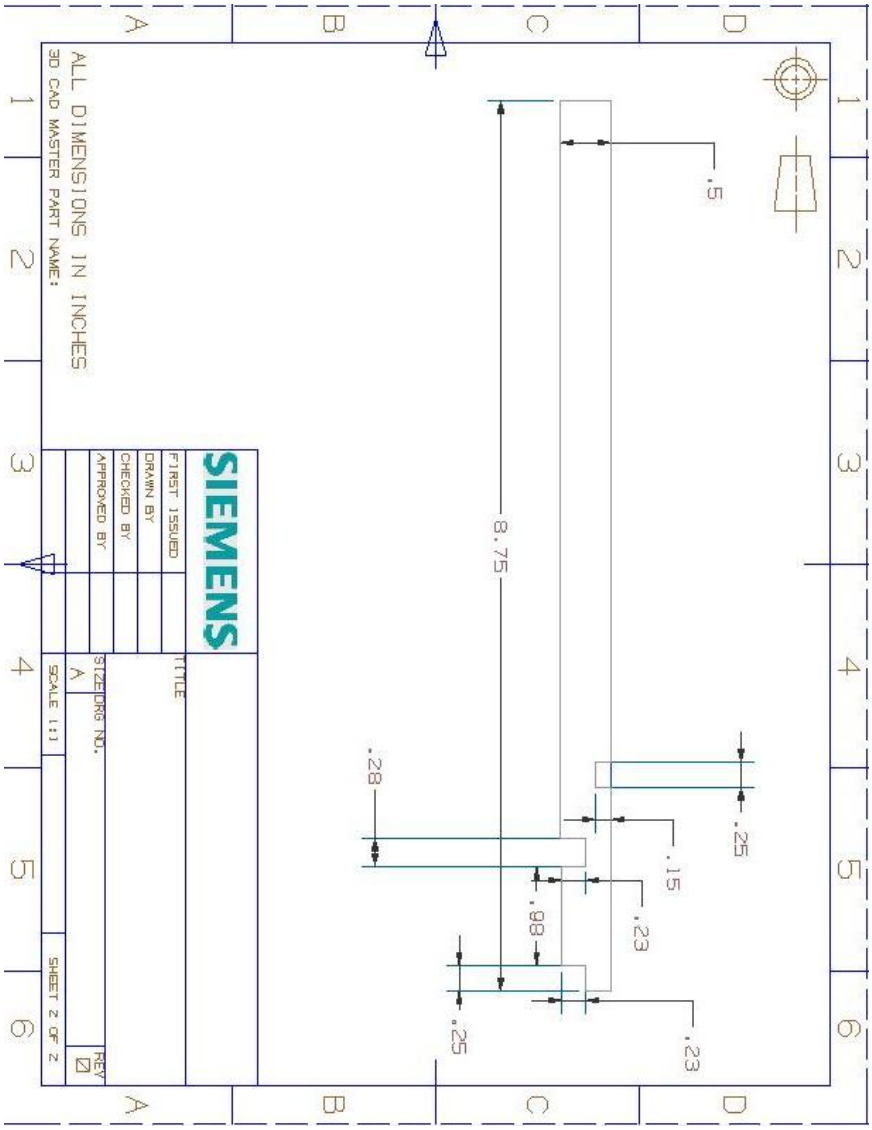

Figure B.8: Thermocouple Flat Plate

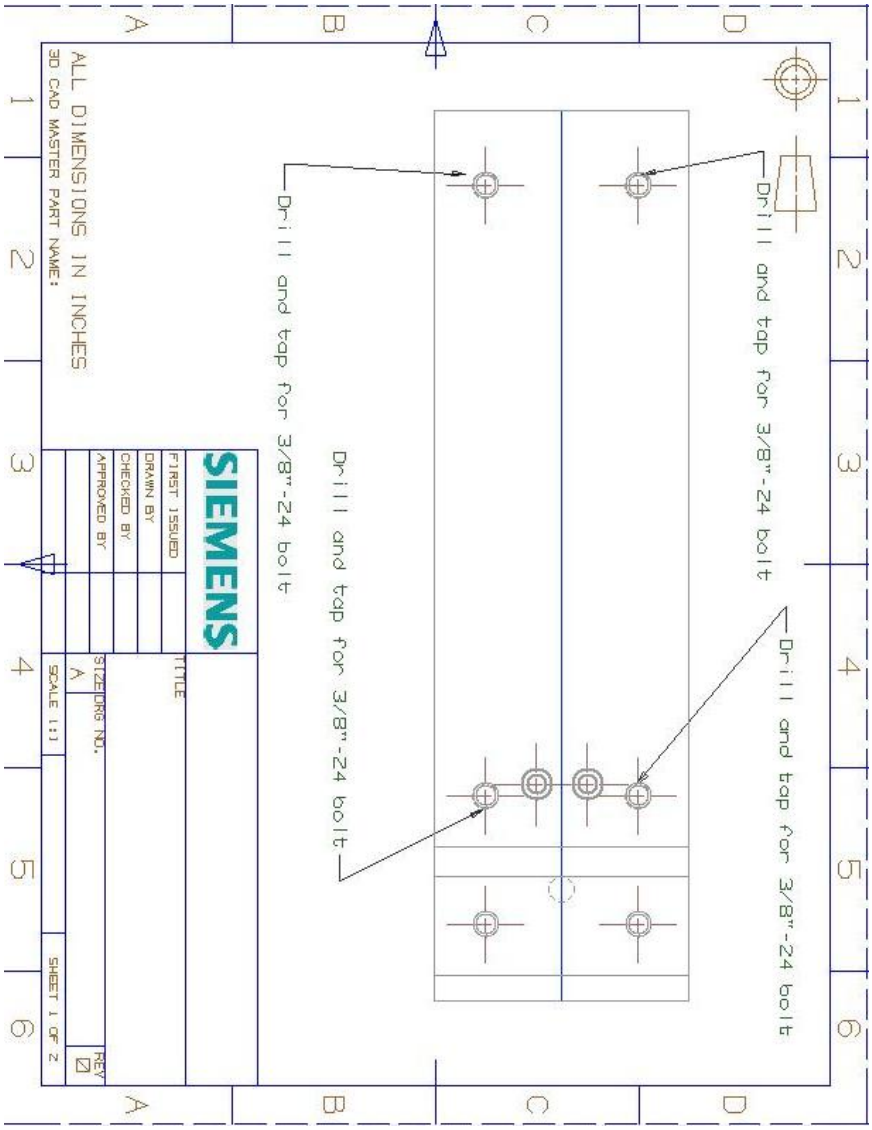

Figure B.9: Thermocouple Flat Plate

Appendix C

Thin Film Flat Plate Drawings

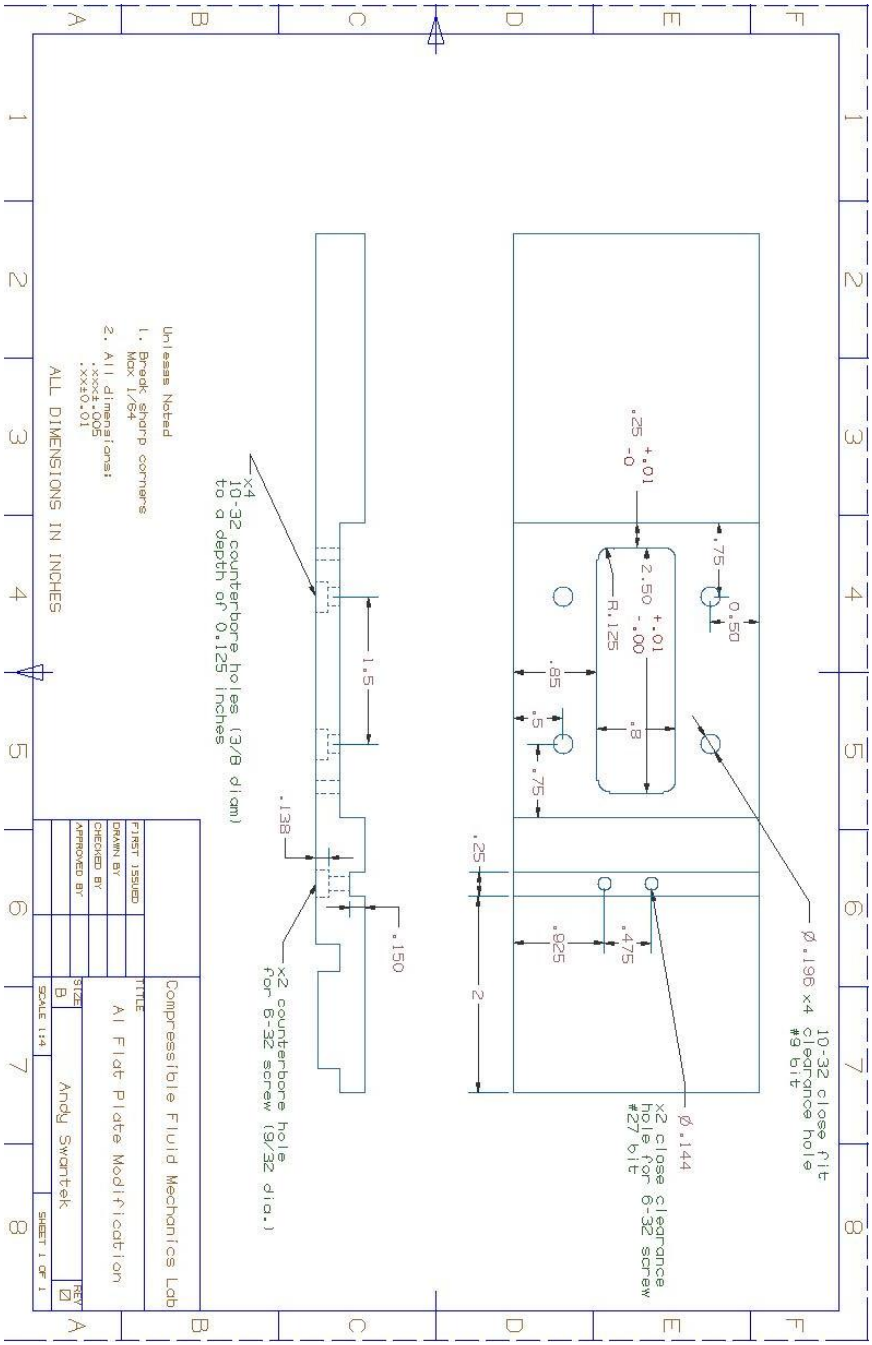

Figure C.1: Thin Film Flat Plate

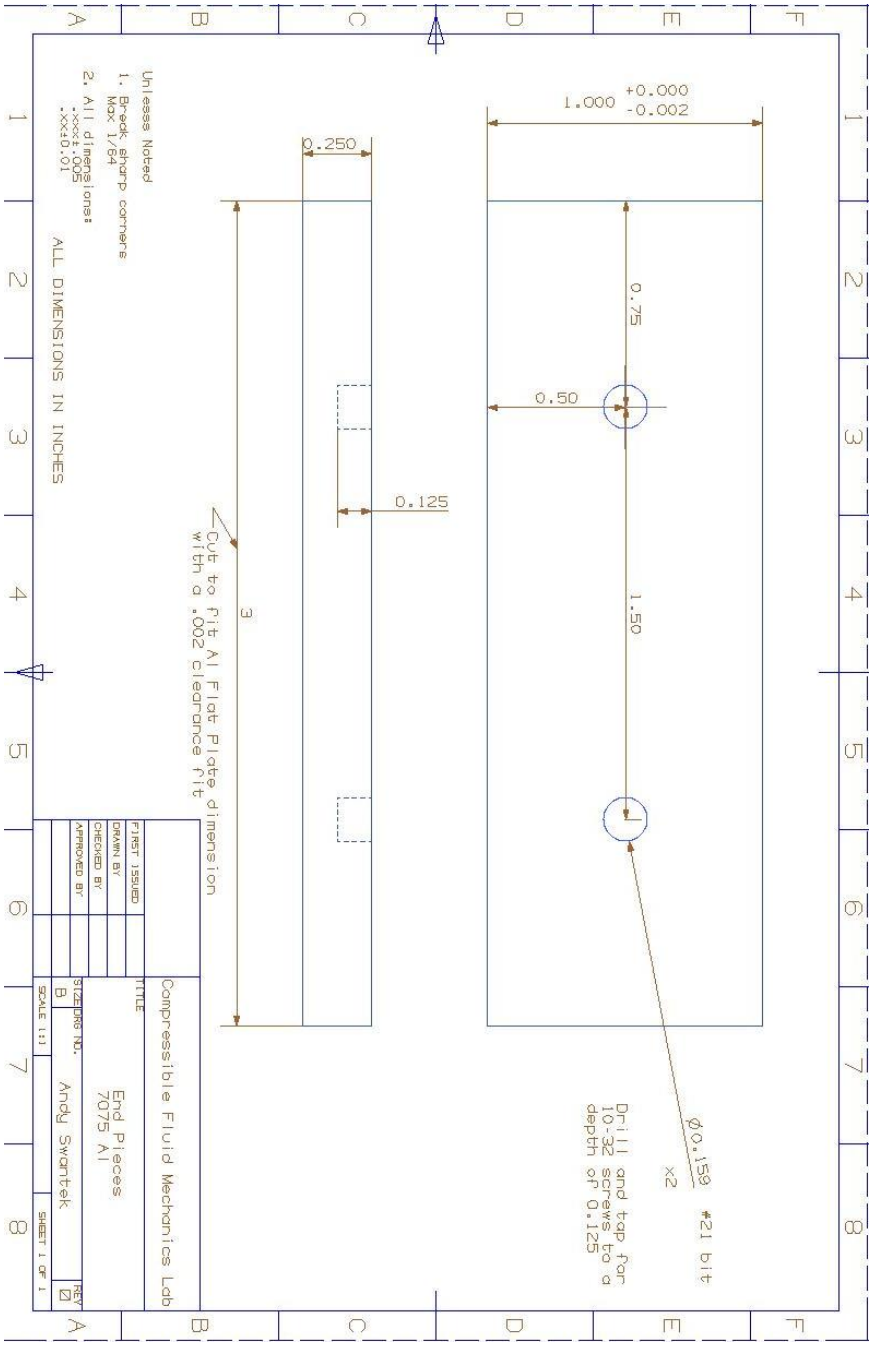

Figure C.2: Thin Film Flat Plate Spacer

Appendix D

Stagnation Model Drawings

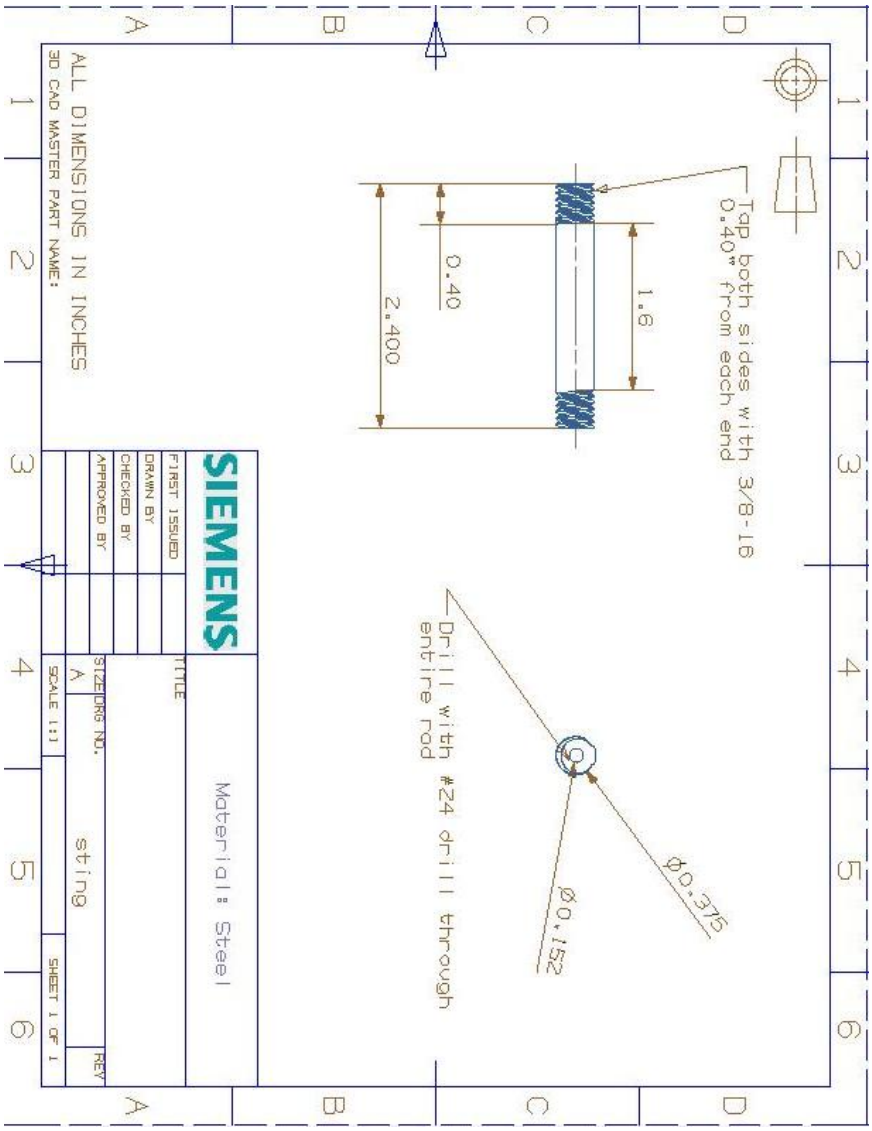

Figure D.1: Stagnation Sphere Mount Sting

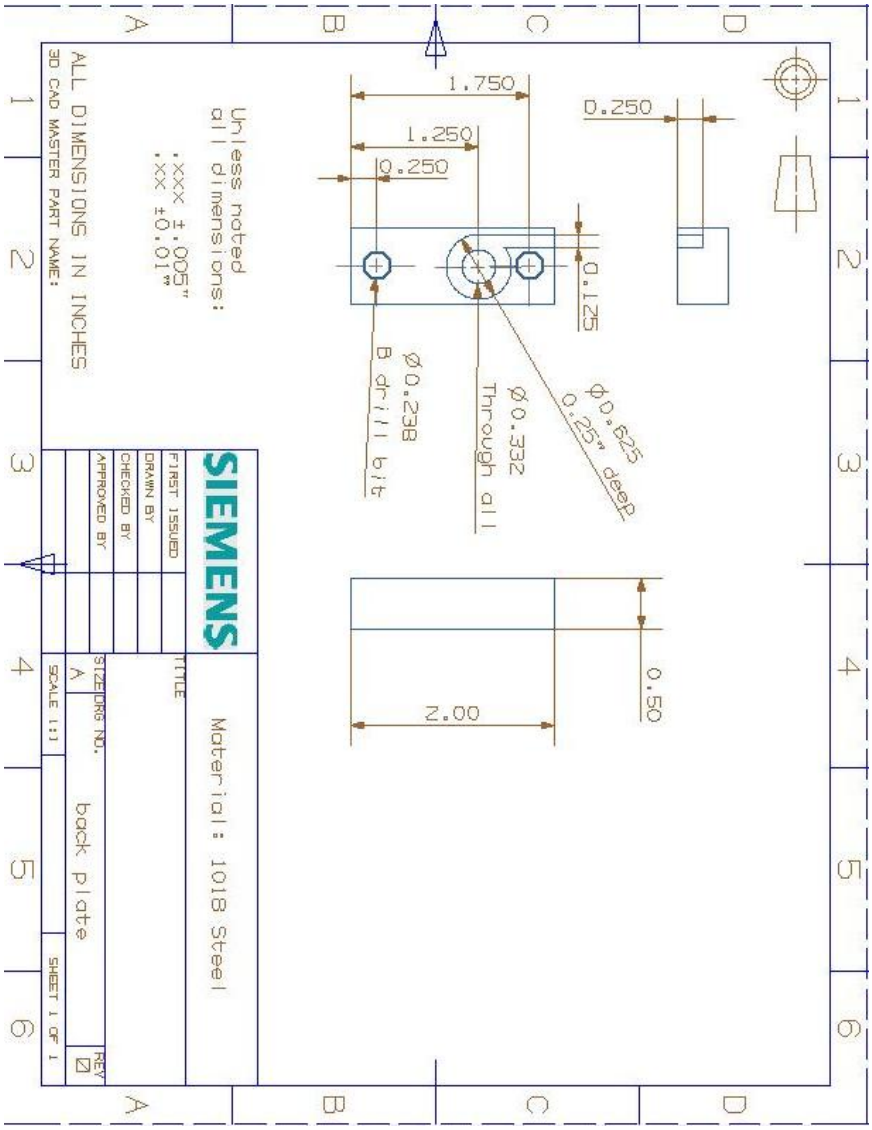

Figure D.2: Stagnation Sphere Backing Plate

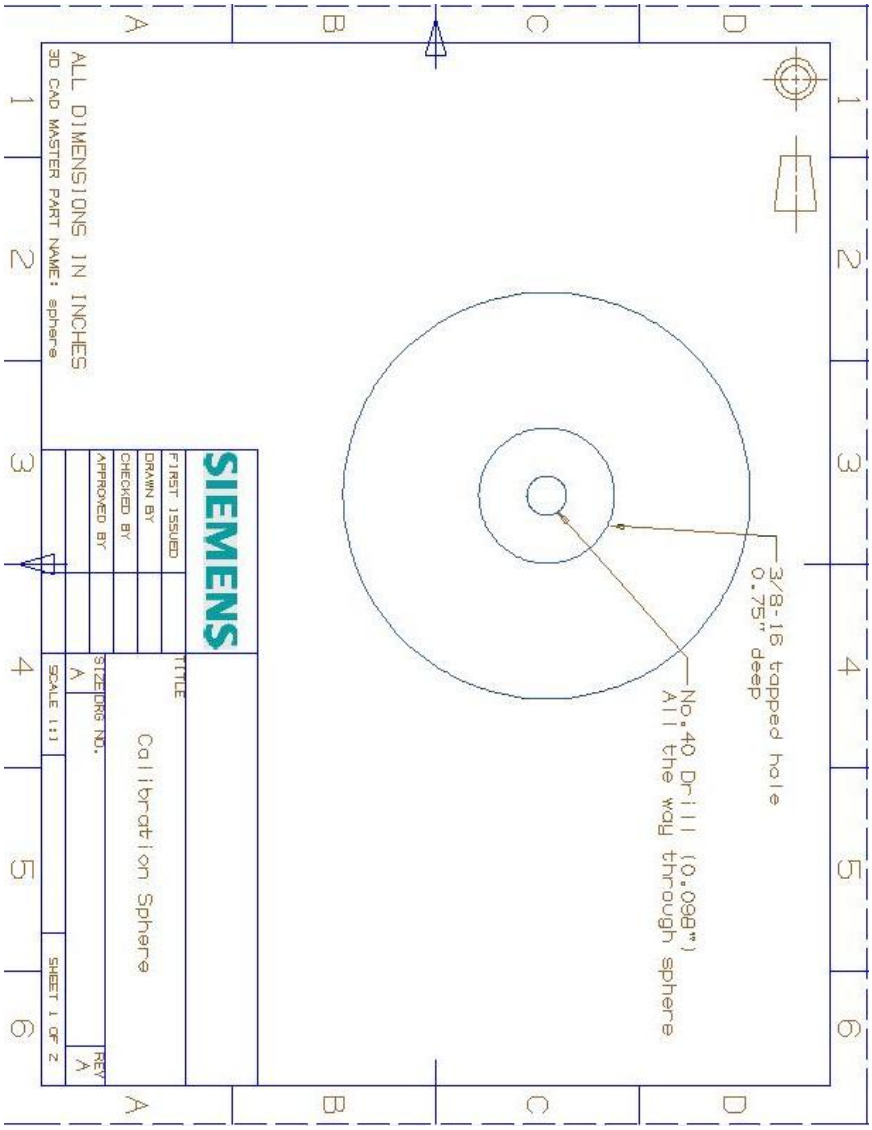

Figure D.3: Stagnation Sphere

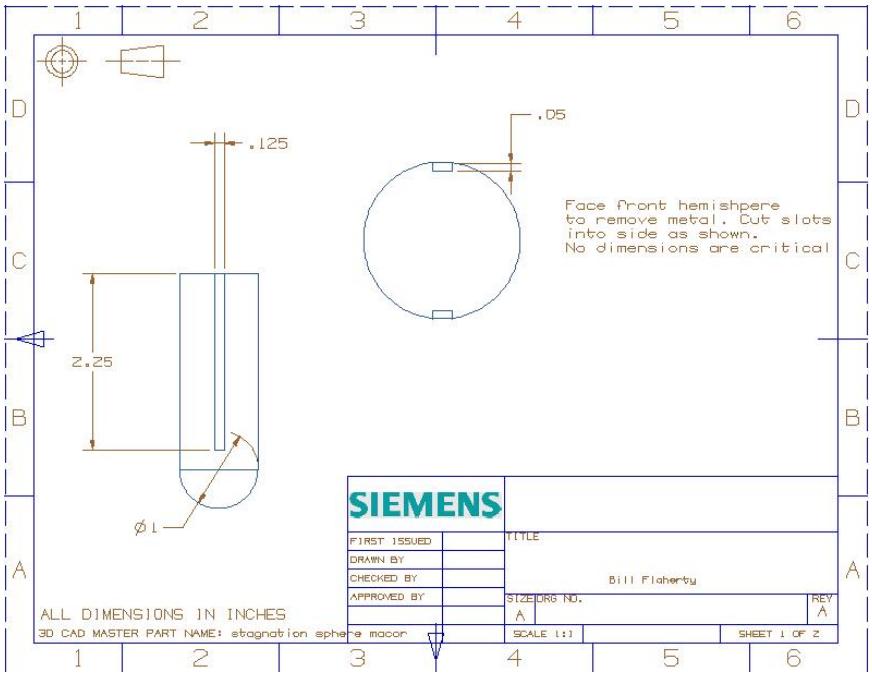

Figure D.4: Thin Film Stagnation Sphere

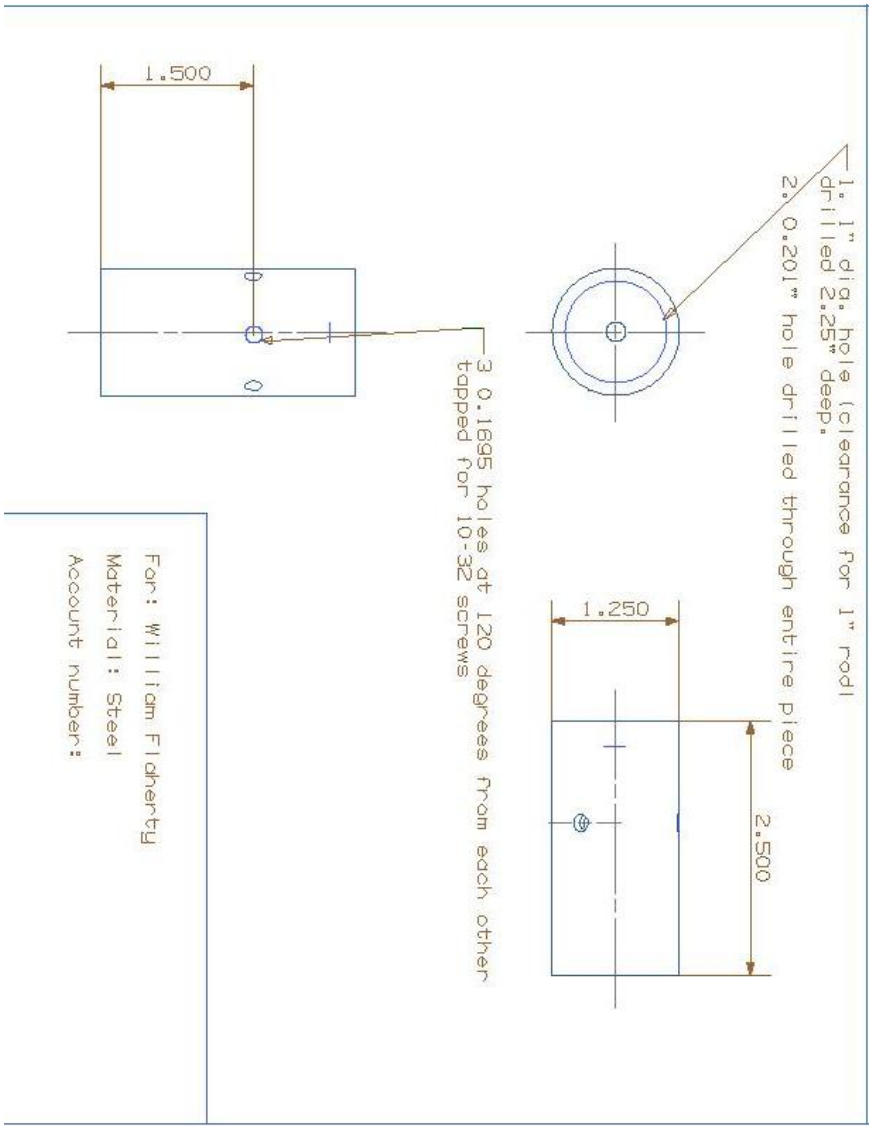

Figure D.5: Thin Film Stagnation Sphere Mount Sleeve

References

[1] Manu Sharma. Further development and experimentation with the hypervelocity expansion tube. Master's thesis, University of Illinois, Urbana, IL, May 2007.

[2] M S. Holden, T P. Wadhams, G J. Smolinski, M G. Maclean, J. Harvey, and B J. Walker. Experimental and numerical studies on hypersonic vehicle performance in the lens shock and expansion tunnels. *44th AIAA Aerospace Science Meeting and Exhibit*, January 2006.

[3] M S. Holden, T P. Wadhams, M G. Maclean, E. Mundy, and R A. Parker. Experimental studies in lens i and x to evaluate real gas effects on hypervelocity vehicle performace. *45th AIAA Aerospace Science Meeting and Exhibit*, January 2007.

[4] M S. Holden, T P. Wadhams, M. Maclean, E. Mundy, and R A. Parker. Experimental studies in lens i and x to evaluate real gas effects on hypervelocity vehicle performance. *45th AIAA Aerospace Sciences Meeting and Exhibit*, January 2007.

[5] M. Maclean and M S. Holden. Catalytic effects on heat transfer measurements for aerothermal studies with co2. *44th AIAA Aerospace Sciences Meeting and Exhibit*, January 2006.

[6] T. Wadhams, E. Mundy, M. Maclean, and Michael Holden. Experimental and analytical study of transition in high speed flows at cubrc. *38th Fluid Dynamics Conference and Exhibit*, June 2008.

[7] Matthew MacLean, Michael Holden, and Brian Hollis. Investigation of blunt bodies with co2 test gas including cataltytic effects. *38th AIAA Thermophysics Conference*, June 2005.

[8] Kenneth M. Chadwick. Stagnation heat transfer measurement techniques in hypersonic shock tunnel flows over spherical segments. *32nd AIAA Thermophysics Conference*, June 1997.

[9] T P. Wadhams, M. Maclean, M S. Holden, and G J. Smolinski. Return to flight testing of a 3.5model at mach numbers of 3.5 and 4.0. *44th AIAA Aerospace Sciences Meeting and Exhibit*, January 2006.

[10] Charles G. Miller. Comparison of thin-film resistance heat -transfer gages with thin-skin transient calorimeter gages in conventional hypersonic wind tunnels. NASA Technical Memorandum 83197, NASA, 1981.

[11] C T. Kidd. Coaxial surface thermocouples: Analytical and experimental considerations for aerothermal heat-flux measurement applications. *Proceedings of the ISA Aerospace Instrumentation Symposium*, 1990.

[12] C T. Kidd, C G. Nelson, and W T. Scott. Extreaneous thermoelectrioc emf effects resulting from press-fit installation of coaxial thermocouples in metal models. *Proceedings of the ISA Aerospace Instrumentation Symposium*, 1994.

[13] Brian R. Hollis, Karen T. Berger, Thomas J. Horvath, Joseph J. Coblish, and Joseph D Norris. Aeroheating testing and predictions for project orion cev at turbulent conditions. *46th AIAA Aerospace Sciences Meeting and Exhibit*, January 2008.

[14] N M. Reddy. Heat-rate measurements over 30 and 40 (half-angle) blunt cones in air and helium in the langley expansion tube facility. NASA Technical Memorandum 80207, NASA, 1980.

[15] Brian R. Hollis, Derek S. Liechty, M J. Wright, M S. Holden, T P. Wadhams, M. Maclean, and A. Dyakonov. Transition onset and turbulent heating measurements for the mars science laboratory entry vehicle. *43th AIAA Aerospace Sciences Meeting and Exhibit*, January 2005.

[16] Simon R. Sanderson. *Shock wave interaction in hypervelocity flow*. PhD thesis, California Institute of Technology, Pasadena, California, 1995.

[17] Jean-Paul Davis. *High-Enthalpy Shock/Boundary-Layer Interaction on a Double Wedge*. PhD thesis, California Institute of Technology, Pasadena, California, 1999.

[18] Adam Rasheed. *Passive Hypervelocity Boundary Layer Control Using an Ultrasonically Absorptive Surface*. PhD thesis, California Institute of Technology, Pasadena, California, 2001.

[19] Ivett A. Leyva. *Shock detachment process on cones in hypervelocity flows.* PhD thesis, California Institute of Technology, Pasadena, California, 1999.

[20] David J. Mee. Boundary-layer transition measurements in hypervelocity flows in a shock tunnel. *AIAA Journal*, 40(8):1542–1548, Aug 2002.

[21] Bianca R. Capra, Penelope Levland, and Richard G. Morgan. Subscale testing of the fire ii vehicle in a superorbital expansion tube. *42th AIAA Aerospace Science Meeting and Exhibit*, January 2004.

[22] Hans G Hornung. Performance data of the new free-piston shock tunnel at galcit. *17th AIAA Aerospace Ground Testing Conference*, July 1992.

[23] K. Hannemann and W H. Beck. *Advanced Hypersonic Test Facilities*, chapter Aerothermodynamics Research in the DLR High Enthalpy Shock Tunnel HEG, pages 205–238. AIAA, Reston, VA, 2002.

[24] Michael S. Holden and R A. Parker. *Advanced Hypersonic Test Facilities*, chapter LENS Hypervelocity Tunnels and Application to Vehicle Testing at Duplicated Flight Conditions, pages 73–110. AIAA, Reston, VA, 2002.

[25] John R. Micol. Langley aerothermodynamic facilities complex: Enhancements and testing capabilities. *AIAA Paper*, 1997.

[26] R G. Morgan. Development of x3, a superorbital expansion tube. *38th AIAA Aerospace Sciences Meeting and Exhibit*, January 2000.

[27] A. Sasoh, Y. Ohnishi, K. Koremoto, and K. Takayama. Operation design and performance of a free-piston-driven expansion tube. *37th AIAA Aerospace Sciences Meeting and Exhibit*, January 1999.

[28] M J. Wright, J. Olejniczak, J L. Brown, H G. Hornung, and K T. Edquist. Modeling of shock tunnel aeroheating data on the mars science laboratory aeroshell. *Journal of Thermophysics and Heat Transfer*, 20(4):641–651, 2006.

[29] Eric Marineau and Hans Hornung. Modeling and calibration of fast-response coaxial heat flux gages. *47th AIAA Aerospace Sciences Meeting*, Jan 2009.

[30] I I. Salvadaor, M A S. Minucci, P G P. Toro, A C. Oliveira, and J B. Channes Jr. Development of surface junction thermocouples for high enthalpy measurements. *American Institute of Physics Beamed Energy Propulsion: Fourth International Symposium*, 2006.

[31] Shigeru Kuchi-ishi, Shigeya Watanabe, Kazuyuki Nakakita, Tadao Koyama, Shuichi Ueda, and Katsuhiro. Comparative heat flux measurments between three hypersonic test facilities at nal. *33rd AIAA Fluid Dynamics Conference and Exhibit*, June 2003.

[32] A. Dufrene, M. Sharma, and J M. Austin. Design and charachterization of a hypervelocity expansion tube facility. *Journal of Propulsion and Power*, 23(6):1185–1193, Nov 2007.

[33] A. Paull and R J. Stalker. Test flow disturbances in an expansion tube. *Journal of Fluid Mechanics*, 245:493–521, December 1992.

[34] P A. Kinzie. *Thermocouple Temperature Measurement*. Wiley-Interscience, 1973.

[35] M Carroll Croarkin, William F Guthrie, George E. Burns, Margaret Kaeser, and Gregory F Strouse. Temperature-electromotive force referance function and tables for the letter-designated thermocouple types based on the its-90. Monograph 175, National Institute of Standard Technologies, 1993.

[36] R G. Adelgren. *Localized Flow Control with Energy Deposition*. PhD thesis, Rutgers University, New Brunswick, NJ, 2002.

[37] Kevin M Kinnear and Frank K Lu. Design, calibration and testing and transient thin film heat transfer gauges. *AIAA Paper*, 1998.

[38] D L. Schultz and T V. Jones. Heat-transfer measurements in short-duration hypersonic facilities. Agardograph 165, AGARD, 1973.

[39] J A. Fay and F R. Riddell. Theory of stagnation point heat transfer in dissociated air. *Journal of the Aeronautical Sciences*, 25(2):73–85, 1958.

[40] K. Sutton and A R. Graves. A general stagnation-point convective-heating equation for arbitary gas mixtures. Technical report, NASA, 1971.

[41] F. De Filippis and M. Serpico. Air high-enthalpy stagnation point heat flux calculation. *Journal of Thermophysics*, 12(4):608–610, 1998.

[42] G. Simeonides. Gerneralized reference enthalpy formulations and simulation of viscous effects in hypersonic flows. *Shock Waves*, 8:161–172, 1998.

[43] E R. Van Driest. Turbulent boundary layers in compressible fluids. *Journal of the Aeronautical Sciences*, 18:145–160, 1951.

[44] Eric Marineau and Hans Hornung. Heat flux calibration of t5 hypervelocity shock tunnel conical nozzle in air. *47th AIAA Aerospace Sciences Meeting*, Jan 2009.

[45] Roop N. Gupta. An analysis of the relaxation of laminar boundary layer on a flat plate after passage of an interface with application to expansion-tube flows. Technical report, NASA, 1973.

[46] Eric Marineau, Stuart J Laurence, and Hans Hornung. Apollo-shaped capsule boundary layer transition at high-enthalpy in t5. *48th AIAA Aerospace Sciences Meeting*, Jan 2010.

[47] S G. Mallinson S L. Gai and N R. Mudford. The boundary layer on a flat plate in hypervelocity flow. *Aeronautical Journal*, April 1996.

[48] S. Mohammadian. Viscous interaction over concave and convex surfaces at hypersonic speeds. *Journal of Fluid Mechanics*, 55(1):163–175, 1972.

[49] J R. Sterrett and J C. Emery. Extension of boundary-layer-seperation criteria to a mach number of 6.5 utilizing flat plates with forward-facing steps. Technical report, NASA, 1960.